

**A NEW APPROACH TO ENHANCE SIGNAL-BACKGROUND-RATIO BY
SMART PULSE MANIPULATION AND TIME-GATED DETECTION:
BREAKING THE LIMIT OF DNA DETECTION**

by

LUCA CERESA

Master of Science, 2020
Texas Christian University
Fort Worth, TX

Master of Science, 2017
Polytechnic University of Milan
Milan, IT

Master of Science, 2017
Instituto Superior Tecnico
Lisbon, PT

Bachelor of Science, 2014
Polytechnic University of Milan
Milan, IT

Submitted to the Faculty of
College of Science and Engineering
Texas Christian University

in partial fulfillment of the requirements for the degree of

Doctor of Philosophy



May 2023

APPROVAL

A NEW APPROACH TO ENHANCE SIGNAL-BACKGROUND-RATIO BY SMART PULSE
MANIPULATION AND TIME-GATED DETECTION: BREAKING THE LIMIT OF DNA
DETECTION

by

Luca Ceresa

Dissertation approved:



Major Professor









For the College

Copyright by

Luca Ceresa

2023

ACKNOWLEDGEMENTS

In the first place, I would like to thank my advisor Dr. Karol Gryczynski, who has been able to motivate me and to guide me through the development of my projects. He has always found a way to make the work enjoyable and in perfect alignment with my own attitudes and taste. Moreover, he has been a very good example from the academic and human point of view. I wish to thank Karol for teaching me how to approach problems in a smart rather than merely meticulous way.

Furthermore, I would like to thank my family. Despite the geographical distance between us, they have constantly supported and encouraged me to proceed towards the achievement of my objectives. Since 2013, when I left my own country to begin my studies abroad, my family has continuously shown constant engagement in participating, even if only virtually, in any activity I attended. I am extremely grateful for all their support, both moral and economic. Nonetheless, I greatly appreciate the huge effort they made in supporting my living in a foreign country, which meant fewer opportunities to spend time together.

Among the members of my family, I want to sincerely thank Sara, who has been for me a constant source of enlightenment and happiness. As a former PhD student, she is aware of all the difficulties that such a career brings, and she has always been able to provide me with the encouragement and the motivation I needed to continue walk towards the summit.

I am grateful for the advice and support of my committee; Dr. Karol Gryczynski, Dr. Anton Naumov, Dr. Hana Dobrovolny, Dr. Sergei Dzyuba and Dr. Rafal Fudala. I really appreciate the effort in considering my work and devoting time to it.

Finally, I am grateful to my fellow students for their advice and moral support. In a special way, I would like to thank Emma Kitchner, Michael Seung and Jose Chavez for their help conducting experiments in the lab and their fundamental contribution in editing the presented PhD thesis work.

TABLE OF CONTENTS

Acknowledgements.....	ii
List of Figures.....	iv
Introduction.....	1
CHAPTER 2: Theoretical considerations.....	8
2.1: <i>Multi Pulse Pumping and Time Gated (MPPTG) detection.</i>	8
2.2: <i>Intensity decays</i>	9
2.3: <i>Time-gating</i>	11
2.4: <i>Pulse pumping</i>	13
2.5: <i>Emission spectra (intensities) detected with pulse pumping</i>	17
2.6: <i>Emission spectra (intensities) detected with pulse pumping and time-gated detection</i>	21
2.7: <i>Detection of DNA via intercalation of EtBr</i>	23
2.8: <i>Spectral characterization</i>	24
CHAPTER 3: Detecting DNA with multi-pulsing and time-gating approach	28
3.1: <i>Selecting the pulse separation</i>	28
3.2: <i>Selecting the time-gating</i>	29
3.3: <i>Experimental verification</i>	32
3.3.1: <i>Ethidium Bromide solutions</i>	32
3.3.2: <i>Pulse generation</i>	33
3.3.3: <i>Results</i>	35
3.4 <i>Summary</i>	40
CHAPTER 4: Using Forster Resonance Energy Transfer to enhance sensitivity and specificity for DNA detection.....	40
4.1: <i>Theory</i>	41
4.2: <i>How FRET can be useful for DNA detection</i>	43
4.3: <i>Experimental results</i>	48
CONCLUSIONS.....	61
References.....	65
VITA	
ABSTRACT	

LIST OF FIGURES

Figure 1: Simulated decays for fluorescence lifetimes of 1ns, 4ns, 10ns, 20ns and 40ns.	10
Figure 2: Simulated decays for fluorescence lifetimes of 1ns, 4 ns, 10 ns, 20 ns and 40 ns with each emitting species contributing with the same total intensity to the observed decay.	11
Figure 3: Intensity decays for 3 ns, 6 ns, and 20 ns lifetimes. A delay for the gate opening (vertical bar) was marked.	12
Figure 4: Total detected signal for the 3 components of 3ns, 6ns and 20ns as a function of the gate opening time, t_g	13
Figure 5: Ratio between long and short components (20ns to 3 ns and 20ns to 6 ns) as a function of gate opening time. The blue line represents the 20 ns to 6 ns ratio multiplied by 10 to improve the trend visibility.	14
<i>Figure 6: Emission intensity decay in a standard single-pulse excitation where the measurement is triggered by the excitation pulse (top). The repetition rate of 2 MHz results in a temporal spacing between pulses of 500 ns (480 ns is indicated as a reference). Intensity decay trace when the excitation is achieved with a burst of four identical pulses with a pulse-to-pulse separation of 10 ns. The additional three pulses in the burst are generated before the first one. As a result, the single pulse is always aligned with the last pulse in the burst.</i>	15
Figure 7: Relative number of molecules in the excited state as function of number of pulses in the burst for three lifetime decays of 3 ns, 20 ns and 50 ns.	17
Figure 8: Simulated normalized emission spectra of background and probe (A) and expected steady-state emission of background, probe and their composition (B).	18
Figure 9: Simulated emission spectra for background, probe, and their composition with 1 and 4 pulses. The differential spectrum obtained by subtracting the signal obtained with 1 pulse from the signal obtained with 4 pulses is reported in purple.	20
Figure 10: Differential spectrum between 4 pulses excitation and 1 pulse excitation normalized to 1 (solid green line). The circles represent the normalized emission spectrum of the probe. The long-lifetime probe has a simulated lifetime of 22 ns and the background presents a simulated lifetime increasing from 1.6 ns, to 2.5 ns, 4 ns, and 6 ns.	21
Figure 11: Expected emission spectra for background (6 ns and 4 ns lifetimes) and probe (22 ns lifetime) with a gate delay of 20 ns and multi-pulsed excitation.	22

Figure 12: Absorption (a) and uncorrected normalized emission (b) spectra of free and DNA-bound EtBr.	25
Figure 13: Expected fluorescence signal measured as a function of EtBr concentration for different concentrations of DNA.	27
Figure 14: Expected number of excited molecules (intensities are proportional to the number of excited molecules) for the long (22 ns) and short (1.6 ns) lifetime components as a function of the number of pulses in the burst.	28
<i>Figure 15: Simulated spectra as expected from the first system (8% bound and 92% free EtBr fractions corresponding to 50:50 intensity between free and bound at 485 nm excitation) single pulse excitation (dashed lines) and 4-pulse excitation (solid lines).</i>	<i>30</i>
Figure 16: Expected emission intensities from the free and bound EtBr fractions as a function of gate time opening for two different concentrations of DNA: 2ng/ μ l (panel A) and 0.3 ng/ μ l (Panel B) after 4-pulse excitation burst. For comparison the top two graphs show intensities observed with single pulse excitation.	31
<i>Figure 17: Schematic representation of the used fiber optics. The fiber splits into 4 equivalent branches, with the length of each branch increasing by about 75 cm.</i>	<i>33</i>
<i>Figure 18: Burst of 4 pulses as measured in time correlated single photon counting (TCSPC) system (DeltaFlex from Horiba Inc.): Ludox scattering (0 fluorescence lifetime) (A), Emission of free EtBr solution (1.5 ns fluorescence lifetime) (B), and Emission from a solution of EtBr that is saturated with DNA (\sim95 ng/μl) (C).</i>	<i>35</i>
<i>Figure 19: Time Resolved Emission Spectra (TRES) as measured with 4 pulses excitation burst after a time delay of 0 ns, 2 ns, 5 ns, and 10 ns after the last pulse in the burst, respectively for three DNA concentrations 2, 0.6 and 0.3 ng/μl (the concentration of EtBr is kept constant for each DNA concentration).</i>	<i>37</i>
<i>Figure 20: Time-delayed images of three wells filled with buffer, EtBr solution, and EtBr solutions with different amounts of DNA. Top left – photography of imaging stage with Teflon cuvette cap with three drilled small wells in the center. Top right – camera image of the cap acquired with the 5X objective utilized for the experiment. Bottom – images collected for different delays of gate opening time for two different amounts of DNA in the right well.</i>	<i>39</i>
Figure 21: Jablonski diagram of electronic states for donor and acceptor, showing the process of FRET.	41

Figure 22: Schematic of the DNA with EtBr and YOYO intercalated. In the figure we included the approximate dimensions for the DNA helix. 45

Figure 23: Expected fluorescence signal measured as a function of YOYO concentration for different concentrations of DNA and EtBr. The concentration of EtBr was varied from 10^{-4} M (A) to 2×10^{-4} M (B) and to 5×10^{-4} M (C). 47

Figure 24: Absorption spectra of intercalators YOYO and EtBr in phosphate buffered saline (PBS), free and bound to DNA. The concentrations of the dyes are arbitrary to achieve a comparable absorption range. 48

Figure 25: Uncorrected emission spectra of YOYO and EtBr in phosphate buffered saline (PBS) without DNA and with DNA observed with a 485 nm excitation diode. The emission spectra are normalized to the signal observed with the DNA. 49

Figure 26: Excitation spectra of YOYO and EtBr as single dyes and mixed, with and without DNA, measured at 520 nm emission (A) and 620 nm emission (B). 50

Figure 27: Emission spectra of DNA saturated EtBr and increasing amounts of YOYO, measured with 535 nm (A) and 485 nm excitation (B). 52

Figure 28: Fluorescence intensity decays for a free YOYO solution, a solution of YOYO with DNA, and a solution of YOYO with DNA to which we added increasing amounts of EtBr. The decays were measured at 520 nm observation (A) and 620 nm observation (B). 54

Figure 29: Emission spectra of EtBr and DNA before and after the addition of YOYO and differential spectrum. 55

Figure 30: Emission spectra of EtBr and EtBr with YOYO with increasing amounts of DNA. In absence of DNA, the addition of YOYO causes no increase in the emission of EtBr. Since the addition of 50pg of DNA, a clear increase in the EtBr signal is visible. 56

Figure 31: Time Resolved Emission Spectra (50 ps time delay to limit excitation pulse contribution) obtained from a solution of EtBr, YOYO and 10 pg/ μ l DNA with a single pulse excitation and a burst of 4 pulses for which the pulse-to-pulse separation was 12.5 ns (80 MHz rep rate). The subtraction between the signal obtained with 4 pulses and 1 pulse is displayed as a dashed line. 57

Figure 32: Emission signal of EtBr, EtBr with DNA and EtBr with DNA and 20 μ l of PBS (A); emission signal of EtBr and EtBr with DNA and 20 μ l of YOYO (B); differential signal obtained by subtraction of the signal without YOYO from the signal obtained with YOYO (C); images obtained from microwells filled with EtBr and DNA (D); images obtained from microwells filled

with EtBr and DNA and EtBr with DNA and YOYO (E); differential image obtained from the subtraction of panel D from panel E (F). 59

Figure 33: Left - concept of evanescent wave (TIRF) excitation. Right – concept of sandwich type DNA hybridization assay enhanced by FRET from intercalator..... 63

INTRODUCTION

Fluorescence spectroscopy has been widely utilized in biomedical diagnostics, real-time visualization of biomedical processes, and imaging (Gryczynski 2020), (Jameson 2014), (Lakowicz 2006), (Valeur B 2012). Its extensive utilization is because of its sensitivity, which originates from a clear separation between excitation wavelength and emission wavelength (wavelength shift between absorption and emission called the Stokes shift). In addition to its high sensitivity, fluorescence also offers an excellent resolution. Both high sensitivity and high spatial resolution make fluorescence a very attractive technology for ultrasensitive detection, biomedical diagnostics, and real-time visualization of biomedical processes (Gryczynski 2020) (Jameson 2014) (Lakowicz 2006) (Valeur B 2012). In fact, fluorescence was the first technology able to detect single molecules and is still the dominant technology in single-molecule spectroscopy (Betzig E 1993) (Moerner WE 1989) (Moerner 2003).

Fluorescence refers to a process that occurs after the absorption of a photon; the excited chromophore releases the absorbed energy after some time in the form of a typically lower energy photon (i.e., longer wavelength) (Jameson 2014), (Lakowicz 2006), (Gryczynski 2020), (Valeur B 2012). Chromophores can relax to the ground state either in a radiative way (emission of a photon) or a non-radiative way. Therefore, the efficiency of the radiative process called quantum yield (QY) is defined as (Jameson 2014), (Gryczynski 2020), (Lakowicz 2006), (Valeur B 2012)

$$QY = \frac{\Gamma}{\Gamma + k_{nr}}, \quad (1)$$

where Γ is the radiative deactivation (decay) rate and k_{nr} represents all possible non-radiative decay rates.

The fluorescence lifetime of a fluorophore is the average time duration between the absorption of the photon and the subsequent emission of the photon. Since the deactivation process is a statistical

phenomenon, the fluorescence lifetime represents the time after which the population of excited chromophores has decreased e times. We can then define a characteristic parameter called fluorescence lifetime τ ,

$$\tau = \frac{1}{\Gamma + k_{nr}}. \quad (2)$$

The deactivation rates are typically very high, in the range of $10^8 - 10^9$, and most fluorophores will present fluorescence lifetimes in the range of only a few nanoseconds. Only a limited number of fluorophores will exhibit fluorescence lifetimes longer than 10 nanoseconds (ns). A few long lifetime fluorophore examples are ADOTA (Maliwal B P 2013), (Sorensen T J 2013), Acridine Orange in the aggregate form (Miyoshi N. 1988), or Ethidium Bromide when intercalated to DNA (Kimball J D 2018), (Hazlett T L 1989). Some solid-state materials like quantum dot-type emitters will also have long emissive lifetimes over 20 ns (May A 2009), (Saviotti 1974). Much longer lifetimes are presented by metal–ligand complexes (Kalayanasundarm 1992), (Juris A 1988), (Tyson D S 1999) (Maliwal B 2001) (MLCs) and some metal clusters, (Raut S L 2014), (Shang L 2011) which offer a fluorescence lifetime from hundreds of nanoseconds to microseconds. Furthermore, lanthanide-based emitters are characterized by lifetimes in the range of milliseconds (Charbonnière 2006), (Leif R 1976), (Jin D 2011), (Liu Y 2013). Finally, a separate case is represented by the process of phosphorescence, which can have very long emission lifetimes extending into the range of seconds (Saviotti 1974), (Gacintov N 1989), (Schlyer B 1994), (Kenry C C 2019).

Any measured fluorescence signal depends on excitation light intensity, fluorophore quantum yield, and the number of available fluorophores (fluorophore concentration). Unfortunately, a typical biological system will contain many components contributing to the overall signal. These include endogenous chromophores that are indispensable constituents of any biological system,

scattering of the excitation light, and frequently Raman scattering of water. Therefore, the high sensitivity of fluorescence is very difficult to translate into real biomedical applications. It has been established that for any sensing/detection modality (fluorescence, NMR, PET, etc.), the problem is neither the signal strength nor the sensitivity of the detector; the problem is the background (Frangioni 2009). In a typical biomedical/physiological sample, a relatively small amount of target molecules is present and mixed with high concentrations of similar molecules and unrelated components that highly contribute to the overall sample signal. This challenge is universal to all biological and medical samples, including forensic samples. Forensic samples are typically randomly collected in the field or crime scene and contain tissue, unprocessed blood, or other physiological fluids. So, in all practical applications, the limiting factor is the signal-to-background ratio (SBR). With the incredible progress in detection technologies and probe development, the possible improvement in sensitivity comes down to “background reduction.” In other words, the fundamental obstacle that any detection had to face historically was the capability of obtaining a high signal-to-background ratio without performing extensive sample purification.

Due to the abundance of processes happening when the excitation light interacts with the sample substance, scientists realized a long time ago that the background is a primary concern for practical diagnostics or imaging applications (Frangioni 2009), (Soubret A 2006), (Richards-Kortum R 1996). As a result, many ideas have been proposed to reduce the background contribution in fluorescence-based detection. For example, much effort has been focused on developing near-infrared (NIR) fluorophores and fluorescent nanomaterials (Daehne S 1998), (Vahrmeijer A L 2013), (Sevick-Muraca 2012). The advantage of moving the detection toward the red/NIR range is that the autofluorescence from biological components and tissue significantly decreases, and a higher penetration depth and sensitivity can be achieved. However, scattering of excitation light, especially Raman scattering (mostly coming from water) remains a significant problem.

Additionally, even if most red/NIR emitters present a good QY, their Stokes shift between absorption and emission spectra is very small, and fluorescence lifetimes are very short. It is thus extremely difficult to distinguish the true emission signal from the excitation light scattering and Raman background. This is why chemi-luminescent (CL) materials usually offer better sensitivity. In fact, the chemi-luminescence signal does not require any excitation light and is generated on optically background-free conditions. Furthermore, a higher penetration depth can be reached (Gross S 2005), (Contag C H 2000), (Zong C 2014), (Bhaumik S 2002). Another approach that has been proposed over the years is the use of two-photon excitation. Such a technique allows for deeper penetration into cellular systems, but autofluorescence background, scattering background, and background from second harmonics remain problematic (Denk W 1990).

This is why significant attention has been devoted to developing long-lifetime fluorescent probes for which fast processes like scattering and fast background emission could be easily separated by time gating (delayed observation) (Maliwal B P 2013), which highly improves the signal-to-background ratio. Unfortunately, regardless of the nature of the emission, a common characteristic of long lifetime emitters is typically a very low brightness, which drastically limits the uses of such probes. This low brightness is dictated by quantum mechanical principles (Strickler S J 1962). The long fluorescence lifetime is typically a consequence of a low probability for photon-fluorophore interaction (very low extinction coefficient) and, consequently, very low QY. However, in spite of the brightness limitation, long-lived probes are increasingly attracting attention and hold great promise for practical imaging and diagnostic applications. An attractive advantage of long-lived probes is the possibility of temporally separate photons emerging from faster processes like scattering, Raman scattering, or typical sub-nanosecond and nanosecond fluorescence (Leif R 1976), (Jin D 2011). By applying a calibrated delay for opening the detection after the excitation pulse (a so-called time-gating approach), we can highly suppress short-lived signals (scattering

and background emission). Since time-gating is a passive approach, there is not only a loss in both the short-lived background and scattering signal but also a small loss in the longer-lived probe signal. Even so, such an approach has proven absolutely successful only for very long fluorescence lifetimes, as observed with lanthanide-based probes where nanosecond delay does not result in a significant loss of already weak probe signals (Leif R 1976), (Jin D 2011).

It is thus necessary to mitigate the low brightness of long-lived weak emitter probes to improve detection sensitivity. In order to do so, we recently proposed an approach based on multi-pulse pumping that greatly increases the observed signal from the long-lived probe as compared to the short-lived background (Shumilov D. 2014). A series of appropriately separated pulses (bursts) allows us to selectively increase the fluorescence signal contribution from the long-lived component of the sample. The pulses are arranged in such a way that each subsequent pulse in the burst reaches the sample when the short-lived component has already decayed, while the long-lived one still has a significant population of molecules in the excited state. As a result, we observe a relative increase in the population of the long-lived dye molecules in the excited state. This phenomenon is commonly referred to as “pumping” (Shumilov D. 2014). The obtained signal increase can be an order of magnitude when long lifetime dyes are used. When using multi-pulse pumping and time-gated detection (MPPTGD), we can increase the detection sensitivity by two orders of magnitude even for relatively short probe lifetimes in the range of 20 ns (Kimball J D 2018), (Chib R 2016). Effectively, we can successfully utilize this technology for practical biomedical imaging, and furthermore, produce almost background-free images using pulsing technology and simple image manipulation. By a smart arrangement of pulse sequences, we create conditions to precisely extract the signal associated with the long-lived component and eliminate the undesired short-lived components, scattering, and background. Reducing the background signal is also extremely beneficial for highly scattering systems like tissue or physiological fluids

where we can highly reduce scattering and diffusing photons leading to a significant increase in the detection depth.

In this Ph.D. thesis, we are presenting a novel approach for signal-to-background ratio enhancement and a possibility for a virtually complete removal of the background signal. We theoretically justify the potential of this new approach and experimentally demonstrate the validity of the proposed technology. Calf thymus DNA system was used as our experimental system. Fluorescence-based DNA detection takes advantage of the high signal enhancement of a dye (called intercalator) upon binding to the DNA. Such signal enhancement is a result of the dye stabilization (reduced water-induced quenching) when it is intercalated between the DNA bases. This chromophore stabilization highly decreases the non-radiative deactivation pathways resulting in a much longer fluorescence lifetime. One of the oldest DNA intercalators, Ethidium Bromide (EtBr), increases its fluorescence lifetime from 1.6 ns when free in the solution to 22 ns when bound to DNA. We show that this change in fluorescence lifetime allows for the highly enhanced detection sensitivity by MPPTGD technology.

Highly increased sensitivity for DNA detection presents a great opportunity for multiple forensic applications. In the forensic field, the main limitation is lack of technology capable of reliably detecting and visualizing sub-nano-grams of DNA without prior sample purification, extraction, and amplification. Using highly magnifying microscopy systems and extremely-well purified samples, the ability to observe/monitor a single DNA strand is feasible (Ceresa L 2021), (Cihlar JC 2022), (Dziak R 2018), (Efcavitch JW 2010). However, deploying an advanced microscopy system in the field is quite impractical. Furthermore, finding highly purified DNA samples in the field is rather unrealistic. Therefore, simple and portable technology capable of high sensitivity and specificity for DNA detection and visualization/imaging is very much needed. This is because DNA is practically invisible, and detecting small unprocessed DNA amounts, such as DNA

collected on swabs or DNA on a surface directly in the field (e.g., touch DNA at a crime scene), is visually impossible. Therefore, a technology that would visualize DNA on various substrates would drastically improve sample collection and reduce workflow. For the last few years, we have been testing and developing various approaches to enhance detection sensitivity based on the fluorescence response of common intercalators (Murata SI 2000), (Neely RK 2011), (Rich RM. 2017), (Rich RM 2014). Now we have been able to combine spectral analysis (Rich RM. 2017), multi-pulse pumping, and time-gated detection (Murata SI 2000), (Neely RK 2011), (Rich RM. 2017), (Rich RM 2014) to highly improve detection/imaging sensitivity. Furthermore, detection utilizing Forster Resonance Energy Transfer (FRET) and signal/image subtraction (Ceresa L. 2021) have been exploited to significantly lower the detection limit for samples containing DNA. Such a combination of approaches allowed us to drastically reduce the required amount of DNA needed for the detection. We have been able to demonstrate that it is possible to detect an amount of DNA as low as 10 pg in an unprocessed/unpurified sample. This detection sensitivity reaches a value within the range of DNA contained in a single human cell, an approach that can revolutionize DNA collection and processing.

CHAPTER 2: THEORETICAL CONSIDERATIONS

2.1: Multi Pulse Pumping and Time Gated (MPPTG) detection.

This thesis demonstrates how the use of multi-pulse pumping and time-gated detection with appropriate signal manipulation can dramatically improve the detection sensitivity of long-lived fluorescence probes. Using a model system constituted of a long-lived dye Ruthenium as a probe (lifetime of ~400 ns) and a short-lived Rhodamine as a fluorescence background (lifetime ~ 3 ns), we demonstrated that we can greatly suppress the dominant Rhodamine signal (Ceresa 2022). For such a large difference in fluorescence lifetimes, we can potentially completely remove the background signal and obtain a dramatic increase in the signal-to-background ratio.

This generic approach can be used for any probe that presents a fluorescence lifetime longer than the lifetimes of various background components. Prior studies of tissue and cellular fluorescence indicated that the lifetimes for the majority of physiological components are below 3 ns, with only a minor contribution of lifetimes between 6-7 ns (Fudala R 2014). As demonstrated earlier (Maliwal B P 2013) using fluorescence probes, such as ADOXA, that present a fluorescence lifetime of 20 ns, the physiological background can be significantly suppressed by multi-pulse pumping and time-gated detection.

Based on this knowledge, we recently realized that with such technology we can significantly increase sensitivity for DNA detection. Fluorescent intercalators drastically increase both intensity and fluorescence lifetime when bound to DNA. One of the first intercalators Ethidium Bromide (EtBr), when bound to DNA, exhibits a fluorescence lifetime of 22 ns, which is much longer than the fluorescence lifetime of EtBr unbound (free) in solution of 1.6 ns (Kimball J D 2018). In the presented dissertation, we demonstrate how we can capitalize on the increased fluorescence lifetime of bound intercalator and highly enhance detection sensitivity for DNA deposited on

various substrates. With a technology based on multi-pulse pumping and time-gated detection, we were able to increase DNA detection sensitivity over 100-fold. We also exploited the potential for Forster Resonance Energy Transfer (FRET) between two different intercalating dyes. Incorporating the FRET-based approach in DNA detection further improves the sensitivity and also increases specificity for detection.

In general, a fluorescence marker bound to a target significantly increases its quantum yield and proportionally increases the fluorescence lifetime. Markers like DAPI or YOYO present a dramatic (few hundreds to thousands) increase of intensity upon binding, and their lifetime increases from a few picoseconds to 2-4 ns.

2.2: Intensity decays

In general, time-resolved fluorescence experiments utilize pulsed laser sources. In the most common approach, Time Correlated Single Photon Counting (TCSPC), the sample is excited with a sequence of single pulses with a fixed repetition rate. It is generally assumed that the intensity decay is a statistical (random) process, and the time-dependent intensity $I(t)$ can be described by a simple exponential function,

$$I(t) = I_0 e^{-\frac{t}{\tau}}, \quad (3)$$

where I_0 indicates the initial intensity, t is a generic time, and τ is the lifetime of the considered fluorophore. An adequate frequency of excitation pulses (called repetition rate) should be used depending on the fluorescence lifetime. The inverse of the repetition rate dictates the time separation between two consecutive pulses. The time separation between two pulses can easily be calculated from the repetition rate in use. For example, when the repetition rate is 10 MHz, the time separation between two pulses is 100 ns. In Figure 1, we present the intensity decays for

fluorescence lifetimes of 1 ns, 4 ns, 10 ns, 20 ns, and 40 ns. The rule in time-resolved measurements (TCSPC) is that the pulse-to-pulse separation should be significantly longer than the fluorescence lifetime (typically more than 3 times) to allow the excited fluorophore to decay to the ground state before the arrival of the next pulse.

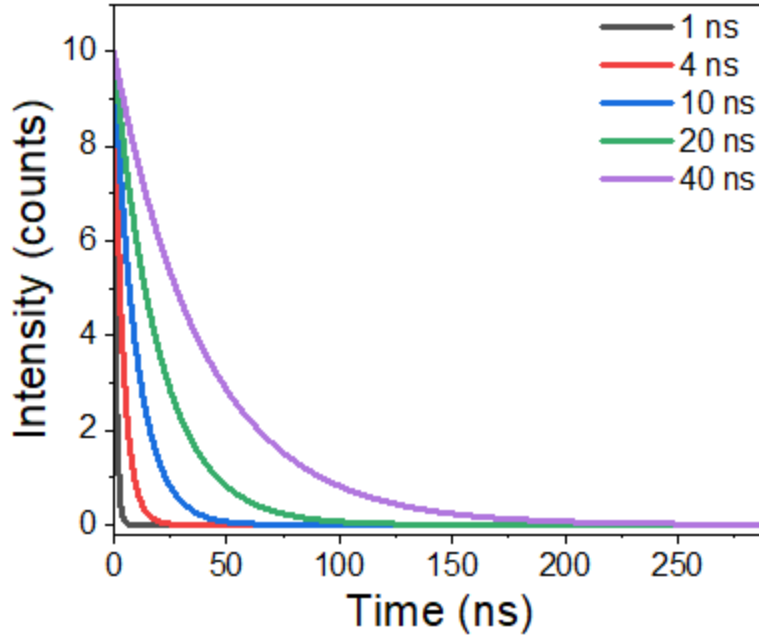


Figure 1: Simulated decays for fluorescence lifetimes of 1ns, 4ns, 10ns, 20ns and 40ns.

It is important to relate the intensity decay to the total observed intensity. For a sufficient separation between pulses, the total intensity (number of collected photons) that corresponds to the so-called steady state intensity is described by

$$I_T = \int_0^{\infty} I(t)dt. \quad (4)$$

In this case, we can consider the intensity decays of different fluorophores contributing to the total intensity (total number of emitted photons). In Figure 2 we present the same decays from Figure 1, but now each emitting species contributes the same total steady state intensity to the observed

decay. It is clear that as the fluorescence lifetime increases, the initial intensity decreases. As a result, the total area under the decay curve (steady state intensity) remains constant.

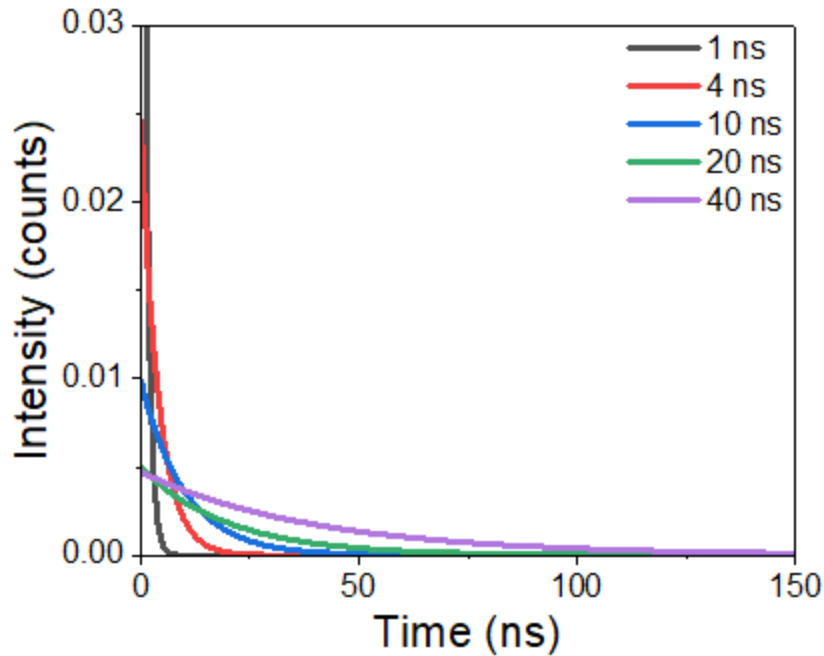


Figure 2: Simulated decays for fluorescence lifetimes of 1 ns, 4 ns, 10 ns, 20 ns and 40 ns with each emitting species contributing with the same total intensity to the observed decay.

2.3: Time-gating

The technique of *time-gating* consists in delaying the gate opening time (delaying the beginning of the detection). In other words, after the pulse is generated, the detector remains closed for a certain portion of time. In Figure 3, we present three intensity decays (3 ns, 6 ns, and 20 ns), where we marked a delay for the gate opening (vertical bar). The gate can be shifted from time zero to any desired time allowed by the pulse separation. For a set gate delay time, the detected signal is obtained only from photons arriving after the gate opening (to the right of the bar in Figure 3), and all photons emitted during the gate delay time are lost (not detected). The total detected signal when applying gating (starting detection after a set time, t_g) is described by

$$I_{t_g} = \int_{t_g}^{\infty} I(t) dt. \quad (5)$$

For convenience in Figure 3 all intensity decays contribute the same steady-state intensities (all species emit the same total number of photons). As a result of the introduced delay, the intensity of the short 3 ns component completely decays before the gate opening times of 20 ns and longer. On the contrary, the intensity of the longer components decays only partially.

As an example, in Figure 4, we schematically present the total detected signal for the 3 components as a function of the gate opening time, t_g . For a 20 ns delay of the gate opening, the short 3 ns component has practically zero detected intensity. For the longer 6 ns component, less than 4% of the intensity is detected, and lastly, for the longest 20 ns component, we can still detect over 35% of the total photons emitted.

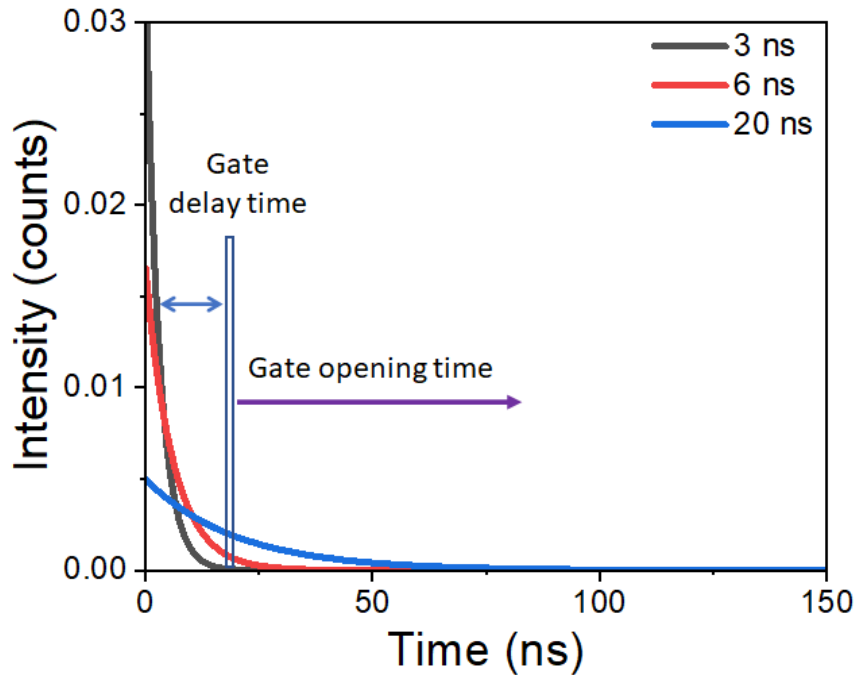


Figure 3: Intensity decays for 3 ns, 6 ns, and 20 ns lifetimes. A delay for the gate opening (vertical bar) was marked.

It is interesting to consider the ratio between long and short components as a function of gate opening time. As shown in Figure 5, the ratio starts from 1 (the total intensities for 0 ns gate delay are equal) and quickly increases to large values. For the 20 ns and 3 ns components, the ratio of

measured intensity after 20 ns approaches 300, and for the 20 ns and 6 ns components after 20 ns is close to 9. It is important to stress that after 20 ns, over 35% of the signal that emerged from the long component can still be detected.

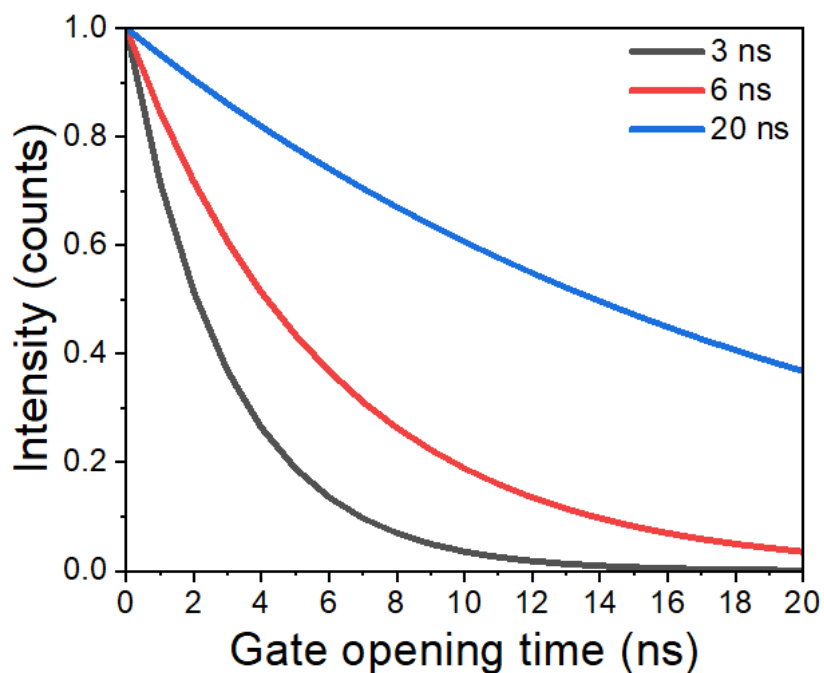


Figure 4: Total detected signal for the 3 components of 3ns, 6ns and 20ns as a function of the gate opening time, t_g .

2.4: Pulse pumping

As mentioned in the introduction, the time-gating approach is a passive approach, and a significant part of the desired signal is lost during the delay of the gate opening. In the presented case in Figure 4, even for a long 20 ns component, 65% of photons are sacrificed. This significantly limits detection sensitivity. Therefore, it would be desirable to increase the signal of the long lifetime component as compared to the signal emerging from the short-lived species. The simplest approach would be to increase the concentration of the long-lived probe. However, this is not

always possible, and in many cases, increasing the concentration of the label (probe) negatively impacts the physiology of the studied object.

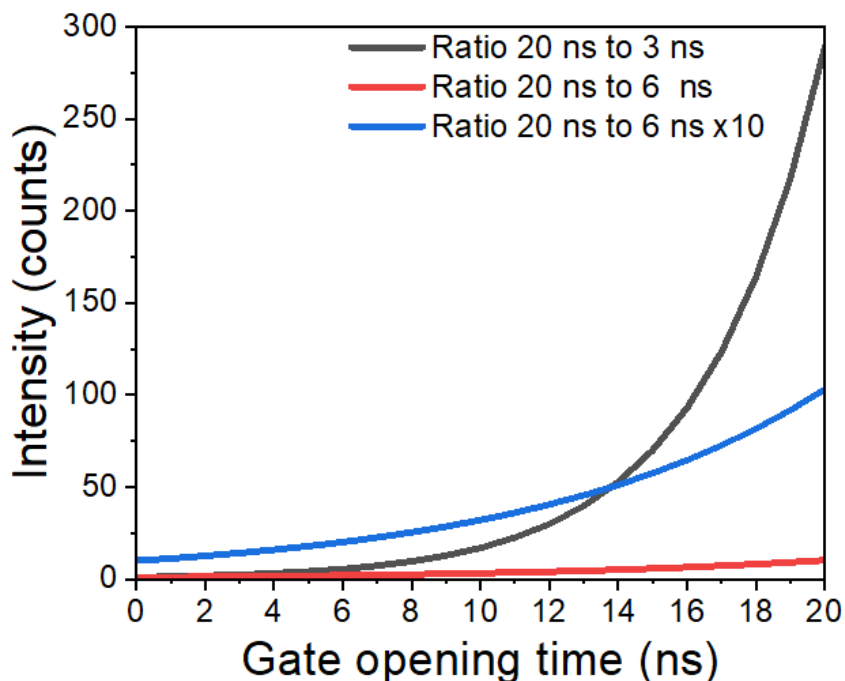


Figure 5: Ratio between long and short components (20ns to 3 ns and 20ns to 6 ns) as a function of gate opening time. The blue line represents the 20 ns to 6 ns ratio multiplied by 10 to improve the trend visibility.

Recently we developed the technology of Multi-Pulse Pumping (MPP) that can significantly increase the initial signal of long-lived probes as compared to the signal of short-lived components. To explain the concept of a multi-pulse pumping approach, let us consider a mixture of two fluorophores that present a short 5 ns fluorescence lifetime and a long 100 ns fluorescence lifetime. In a Time Correlated Single Photon Counting (TCSPC) experiment (a typical time-resolved experiment), the sample is excited with a sequence of single pulses with a fixed repetition rate. In Figure 6 (top), we present an example of sample excitation with a repetition rate of 2 MHz, where the pulse-to-pulse separation is 500 ns.

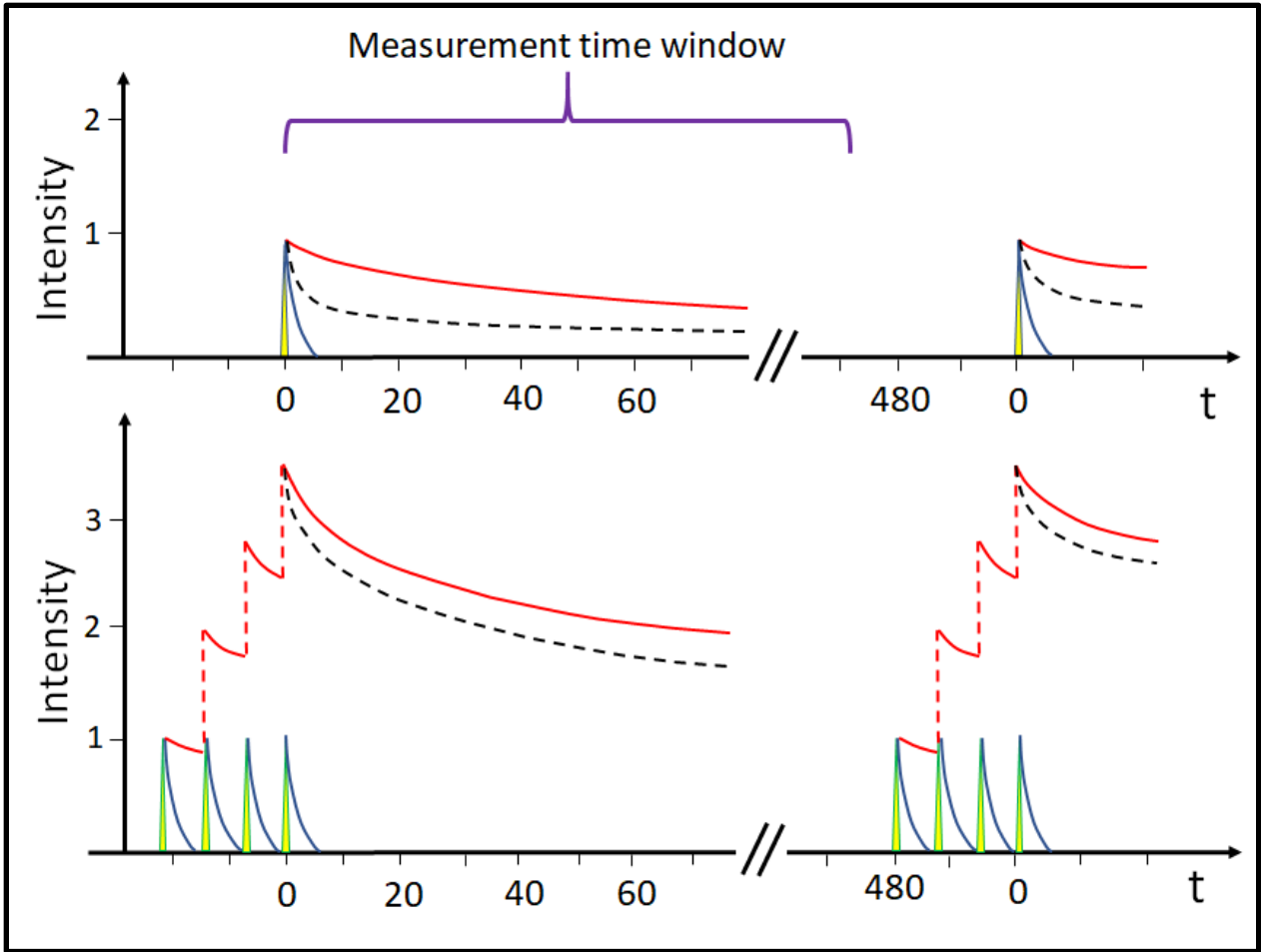


Figure 6: Emission intensity decay in a standard single-pulse excitation where the measurement is triggered by the excitation pulse (top). The repetition rate of 2 MHz results in a temporal spacing between pulses of 500 ns (480 ns is indicated as a reference). Intensity decay trace when the excitation is achieved with a burst of four identical pulses with a pulse-to-pulse separation of 10 ns. The additional three pulses in the burst are generated before the first one. As a result, the single pulse is always aligned with the last pulse in the burst.

This time is sufficient for both short (3 ns) and long (100 ns) components to decay completely. As shown in Figure 6 (top), the short component (blue line) decays very quickly, while the decay of the long component (red line) extends to a much longer time. A black dashed line presents the signal observed from a mixture of the two components. Now, let us assume that the excitation is by a burst of 4 identical pulses separated by 10 ns. Such separation of 10 ns is sufficient for the short lifetime component to almost completely decay. However, during the 10 ns, the long

component will only partially decay, and most of the excited molecules will still be in the excited state when the next pulse arrives. More precisely, the separation of pulses in the burst must be such that each subsequent pulse reaches the sample when the short-lived component has fully decayed and only a small fraction of the long-lived molecules has decayed, while a significant fraction of long-lived molecules is still in the excited state. As a result, the relative contribution of the long-lived molecules is enhanced. At the same time, the short-lived component remains unaltered because any subsequent pulse arrives when all the molecules are already in the ground state. The separation between the bursts is significantly longer than the lifetime of long-lived molecules, allowing the population of all excited molecules to decay to the ground state completely. Therefore, the following sequence of pulse burst starts with all molecules in the ground state.

By triggering the TCSPC detection with the last pulse in the burst, the starting population of long-lived molecules is much higher than with a single pulse, and the population of short-lived molecules is constant. In practice, for a fluorophore with a certain fluorescence lifetime τ , the number of excited molecules after n consecutive excitation pulses in the burst can be described by (Chib R 2016), (Gryczynski 2020)

$$N(\tau, n, RR) = N_e \frac{1 - e^{-\frac{n}{\tau * RR}}}{1 - e^{-\frac{1}{\tau * RR}}}, \quad (6)$$

where RR is the repetition rate in the pulse burst, n is the number of pulses, and N_e is the number of molecules excited by a single pulse.

In Figure 7, we present the relative number of molecules in the excited state as a function of the number of pulses in the burst. The population of long-lived molecules highly increases, and the population of short-lived molecules (3 ns or shorter) is unchanged. In practice, we can increase the population of the long-lived fraction a few folds, while the short-lived population stays constant, by applying a sequence of excitation pulses.

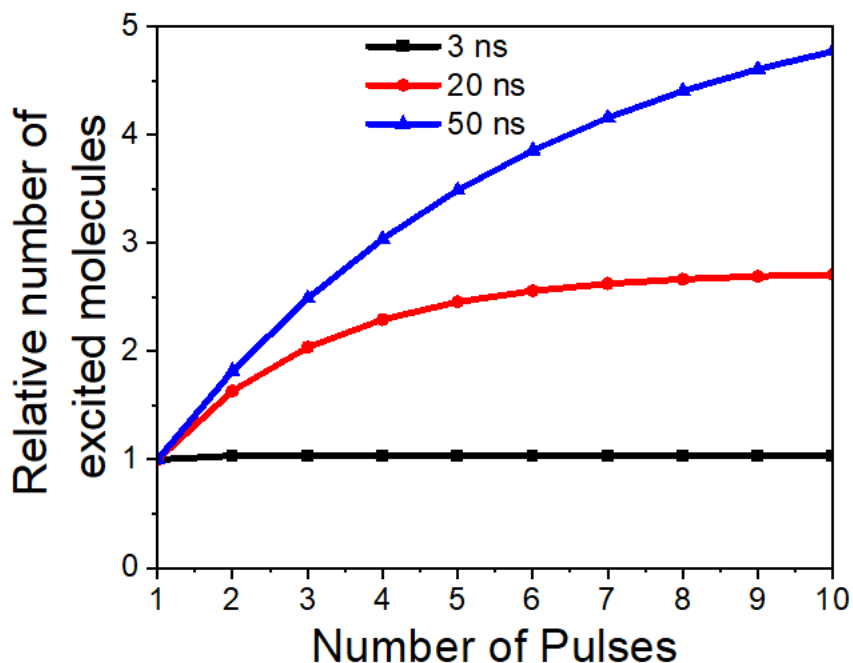


Figure 7: Relative number of molecules in the excited state as function of number of pulses in the burst for three lifetime decays of 3 ns, 20 ns and 50 ns.

2.5: Emission spectra (intensities) detected with pulse pumping

Figure 7 shows that by using 3 or more pulses for excitation, the signal of the long-lifetime component of 20 ns can be doubled, while the signal of the short-lived component remains unchanged. This opens new possibilities for deconvoluting the emission spectrum of long-lived probes from a short-lived background. To demonstrate such a possibility, let us consider the intensity decay of a system that consists of two components: a background that has a short fluorescence lifetime τ_s (e.g., ~1.6 ns that corresponds to lifetime of free – unbound EtBr in solution) and is characterized by a broad single emission band (Gaussian) with a single maximum at 550 nm, and a probe that is characterized by a long fluorescence lifetime τ_l (e.g., 22 ns that corresponds to the lifetime of EtBr bound to DNA). The simulated normalized emission spectra of the background (black) and probe (red) are reported in Figure 8(A). To make the reasoning clear,

the probe emission has two peaks at 540 and 630 nm to be easily distinguished from the background emission, as presented in Figure 8(A).

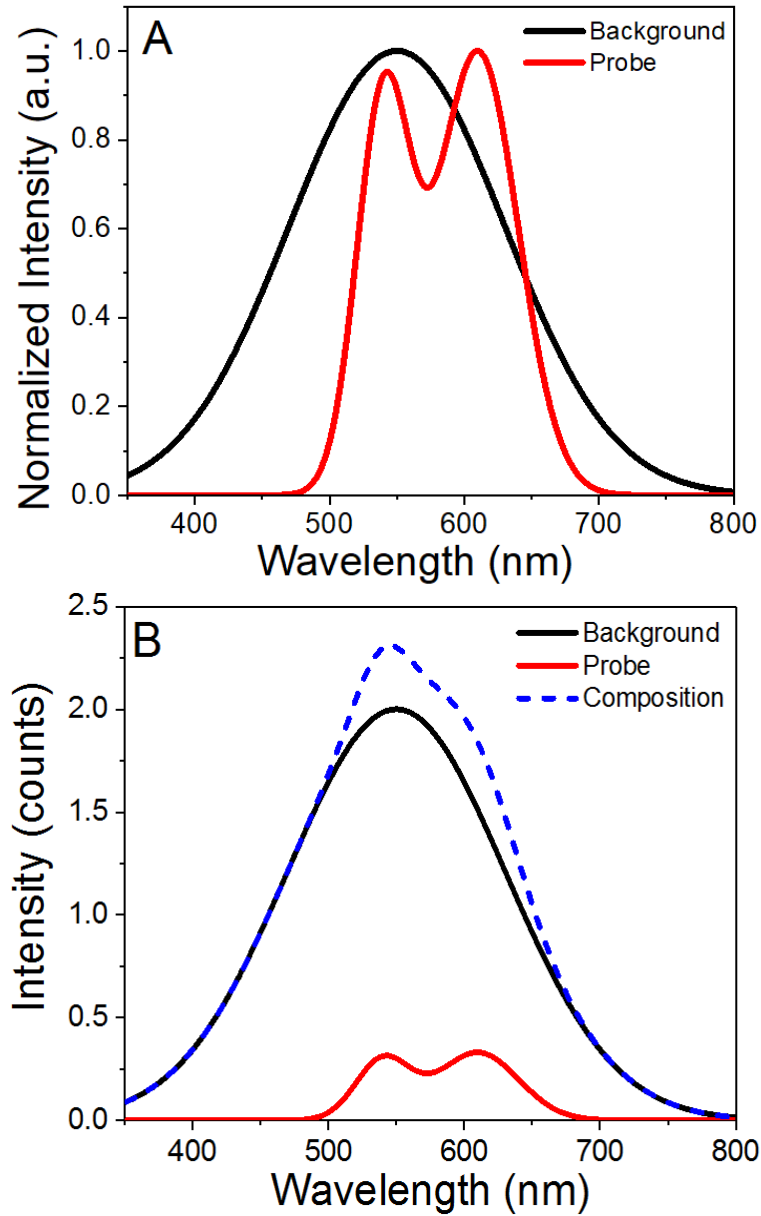


Figure 8: Simulated normalized emission spectra of background and probe (A) and expected steady-state emission of background, probe and their composition (B).

In this example, we assume that the background emission is about 10 times stronger than the probe signal and overlays the entire probe emission. The expected steady-state emission of the background, probe and their composition are presented in Figure 8(B). The expected cumulative emission from the probe and background is presented as a blue dashed line in Figure 8(B). Since we assumed that the background contribution to the steady-state intensity is 10 times greater, the cumulative emission is entirely dominated by the background. In cases where the emission spectra are known, the cumulative emission can be precisely decomposed to separate background and probe components. However, if a spectrum is unknown (a frequent case with background emission), the deconvolution will not produce satisfactory results. Also, from the point of view of imaging, a large background contribution that is comparable to or larger than the probe signal would disqualify any image analysis.

Let us assume the system in Figure 8B is excited with a burst of 4 identical consecutive pulses separated by 10 ns, and the detection starts with the last pulse, as schematically shown in Figure 6. The new expected intensities calculated according to Equation (6) are presented in Figure 9. The short-lived background signal did not change, and the long-lived probe signal (dashed red) increased over two times compared to the signal observed with a single pulse excitation. The cumulative signal (blue dashed line) indicates the increased contribution of the structured emission (long-lived probe). For convenience, in Figure 9, we also included the probe signal measured with a single pulse excitation (dashed yellow line). The difference between the cumulative signal with 4 pulses excitation and the cumulative signal with a single pulse excitation is presented as a solid purple line. This represents the probe signal increase after 4 pulses, which is greater than the probe signal with just a single pulse.

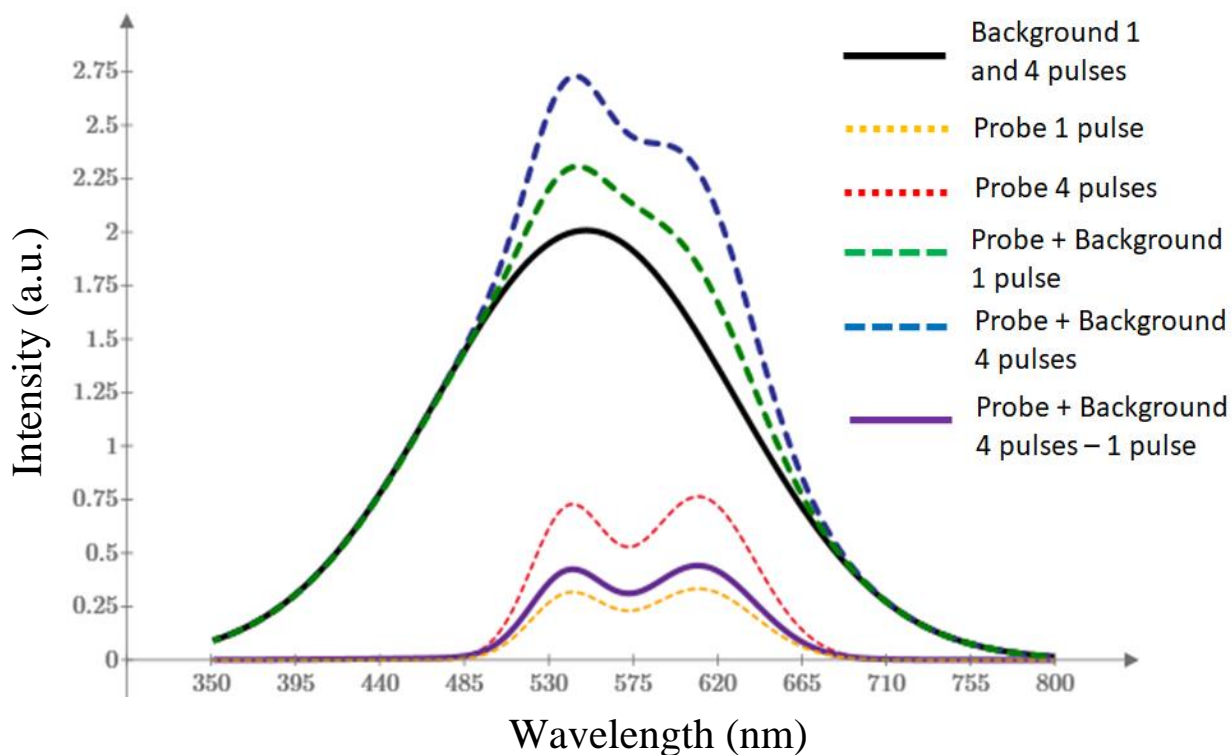


Figure 9: Simulated emission spectra for background, probe, and their composition with 1 and 4 pulses. The differential spectrum obtained by subtracting the signal obtained with 1 pulse from the signal obtained with 4 pulses is reported in purple.

When we compare Figure 8B and Figure 9, we see the observed difference is solely associated with the signal increase due to the pulsed excitation. In this case, we can construct a simple difference between the spectrum measured with four-pulse excitation and the spectrum measured with a single-pulse excitation. Figure 10 presents such difference normalized to 1 as a solid line. The circles represent the normalized emission spectrum of the probe. The long-lifetime probe has a simulated lifetime of 22 ns, and the background presents a simulated lifetime increasing from 1.6 ns to 2.5 ns, 4 ns, and 6 ns. For a background lifetime of 1.6 ns (or shorter), the differential spectrum perfectly reflects the long-lived component spectrum. As the fluorescence lifetime of the background increases, we start to also pump the background component, and the recovered

differential spectrum contains some background. However, even for a background lifetime of 6 ns, the long-lived probe spectrum is the dominant component.

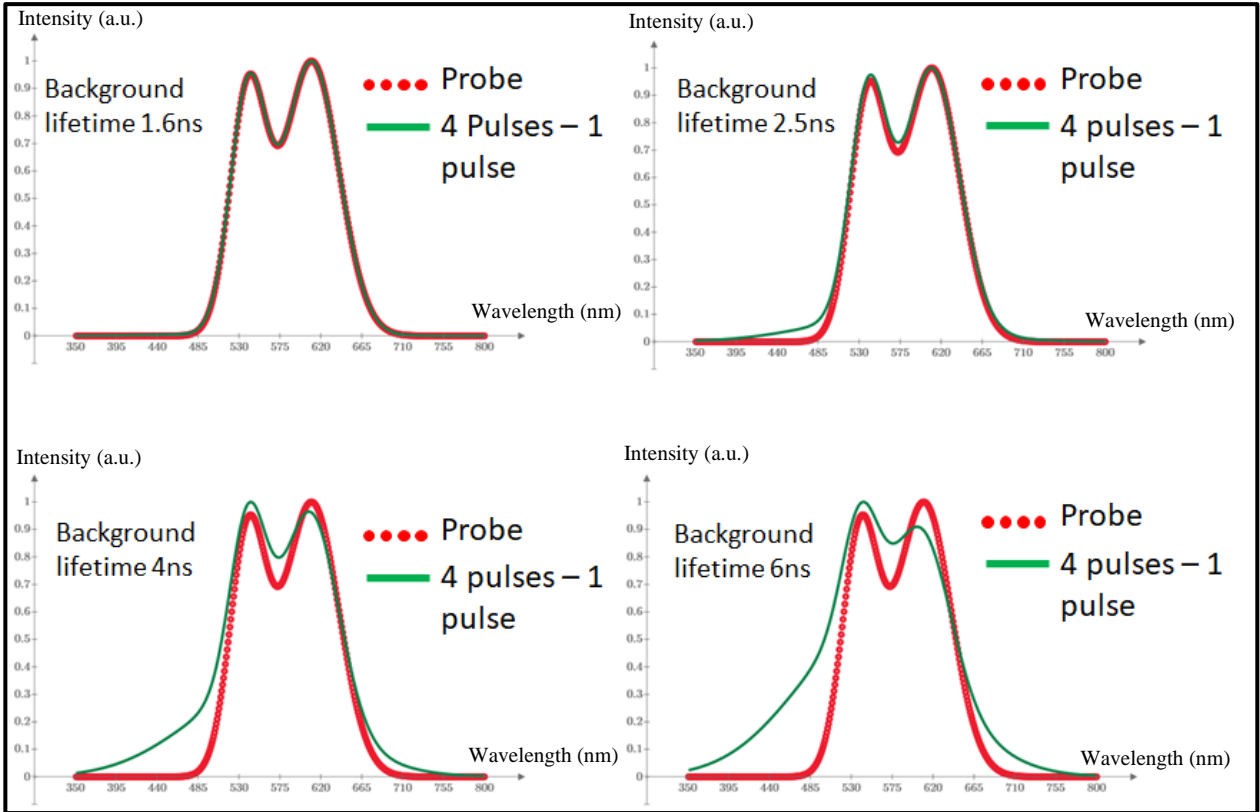


Figure 10: Differential spectrum between 4 pulses excitation and 1 pulse excitation normalized to 1 (solid green line). The circles represent the normalized emission spectrum of the probe. The long-lifetime probe has a simulated lifetime of 22 ns, and the background presents a simulated lifetime increasing from 1.6 ns, to 2.5 ns, 4 ns, and 6 ns

2.6: Emission spectra (intensities) detected with pulse pumping and time-gated detection

The important conclusion from Figure 9 and Figure 10 is a significant increase in the long-lived probe signal. After 4 pulses, the signal of the long-lived probe increases 2.4 times. The enhanced signal of the probe opens a possibility for time-gated detection.

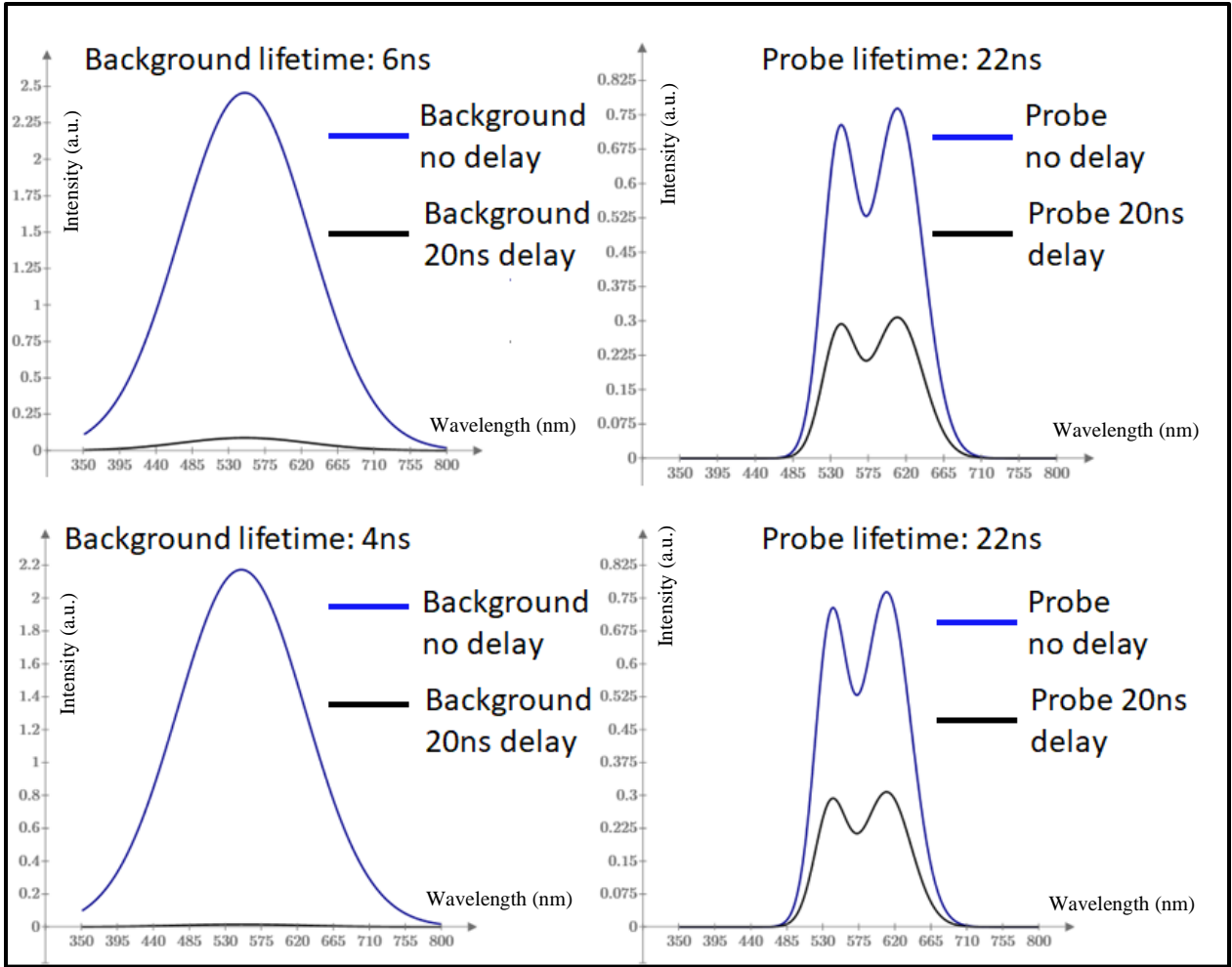


Figure 11: Expected emission spectra for background (6 ns and 4 ns lifetimes) and probe (22 ns lifetime) with a gate delay of 20 ns and multi-pulsed excitation.

In Figure 11, we present the expected emission spectra for a gate delay of 20 ns. For a lifetime of 22 ns, after 20 ns, the intensity decreases about 2.4-fold. Therefore, the initial intensity for the long component will be equal to that expected from a single pulse, however the short-lived background component decreases much more. For a background lifetime of 6 ns, we can still detect a small trace of background, but the signal is much smaller than in the regular single pulse excitation mode without gating. The background contribution becomes negligible for a background lifetime of 4 ns, and for shorter lifetimes, it is not detectable.

In conclusion, the overall detected signal from the probe excited with the burst of pulses is significantly greater than the signal detected with single-pulse excitation. Furthermore, the differential spectrum well reflects the emission spectrum of the long-lived component (probe). Additionally, any noise and ambient signals are eliminated by the spectra subtraction. This creates a great opportunity for image manipulation/enhancement during typical imaging in the field.

2.7: Detection of DNA via intercalation of EtBr

The considerations/simulations discussed above clearly indicate the possibility of enhancing the signal from a probe that presents a fluorescence lifetime longer than 20 ns with respect to the short-lived background emission. A common DNA intercalator EtBr when free in solution (water buffer), presents a fluorescence lifetime of 1.6 ns, typically a main background component. When bound to DNA, its fluorescence lifetime increases to 22 ns. This presents a great opportunity to apply the proposed pulse-pumping and time-gating technology to highly enhance DNA detection sensitivity.

The ability to detect and visualize traces of DNA present in a sample has an immediate and fundamental benefit for the forensic industry and crime investigations. Specifically, according to the normal forensic procedure, any crime scene is swabbed with cotton or polyester-based swabs. The DNA contained in the swabs is then subjected to a polymerase chain reaction (PCR), with the aim of multiplying the DNA fragments and identifying the DNA sequence that is highly specific for each individual. The important initial requirement for successful DNA amplification is to accumulate/collect a sufficient starting amount of DNA. With the current PCR technology, the minimum standard amount is about 1 ng of DNA (K. K. Kanokwongnuwut P. 2018), (K. P. Kanokwongnuwut P. 2018), (Comte J. 2019). Unfortunately, not all the swabs utilized on the crime scene collect enough DNA fragments to ensure a successful amplification and provide useful

information. On the contrary, sometimes forensic laboratories must deal with swabs that contain an insufficient amount of DNA or no DNA at all. This makes the entire procedure of DNA identification lengthy and expensive. Therefore, it is tremendously important to develop a reliable pre-screening technique, to successfully identify the presence of DNA in the field and directly on the swabs. Such a technique could provide guidance for swabbing areas and help exclude useless swabs, saving resources and time.

We applied the multi-pulsing and time-gated detection approach to highly enhance the detection limit of minute amounts of DNA. We demonstrate the potential value of the proposed approach to minimize the detectable amount of DNA first in solution and then directly on swabs.

2.8: Spectral characterization

Binding a dye/chromophore to DNA results in a significant change of the surrounding/ environment of the dye. In the specific case of EtBr, and generally for many other intercalators, the chromophore is transferred from a highly polar water environment to a much less polar environment (between the DNA bases, where water access is limited).

As a result, when EtBr intercalates into DNA, the dye is stabilized (less quenched), and the nonradiative deactivation rate decreases, resulting in a higher quantum yield and a longer fluorescence lifetime. Also, such environment stabilization between the DNA bases produces minor changes in the absorption and emission spectra. Figure 12 shows the absorption spectrum and the uncorrected normalized emission spectra of free EtBr and EtBr fully bound to DNA. The absorption spectrum slightly shifts to the red when bound to DNA, and the emission spectrum of EtBr bound to DNA shifts toward the blue (shorter wavelength) compared to a free EtBr in solution. Moreover, it is important to emphasize that the fluorescence signal of the bound EtBr is

about 6 times greater with 485 nm excitation (QY increases about 15 times (Fritz M.P. 1972)). As a result, the emission of the bound form is significantly enhanced.

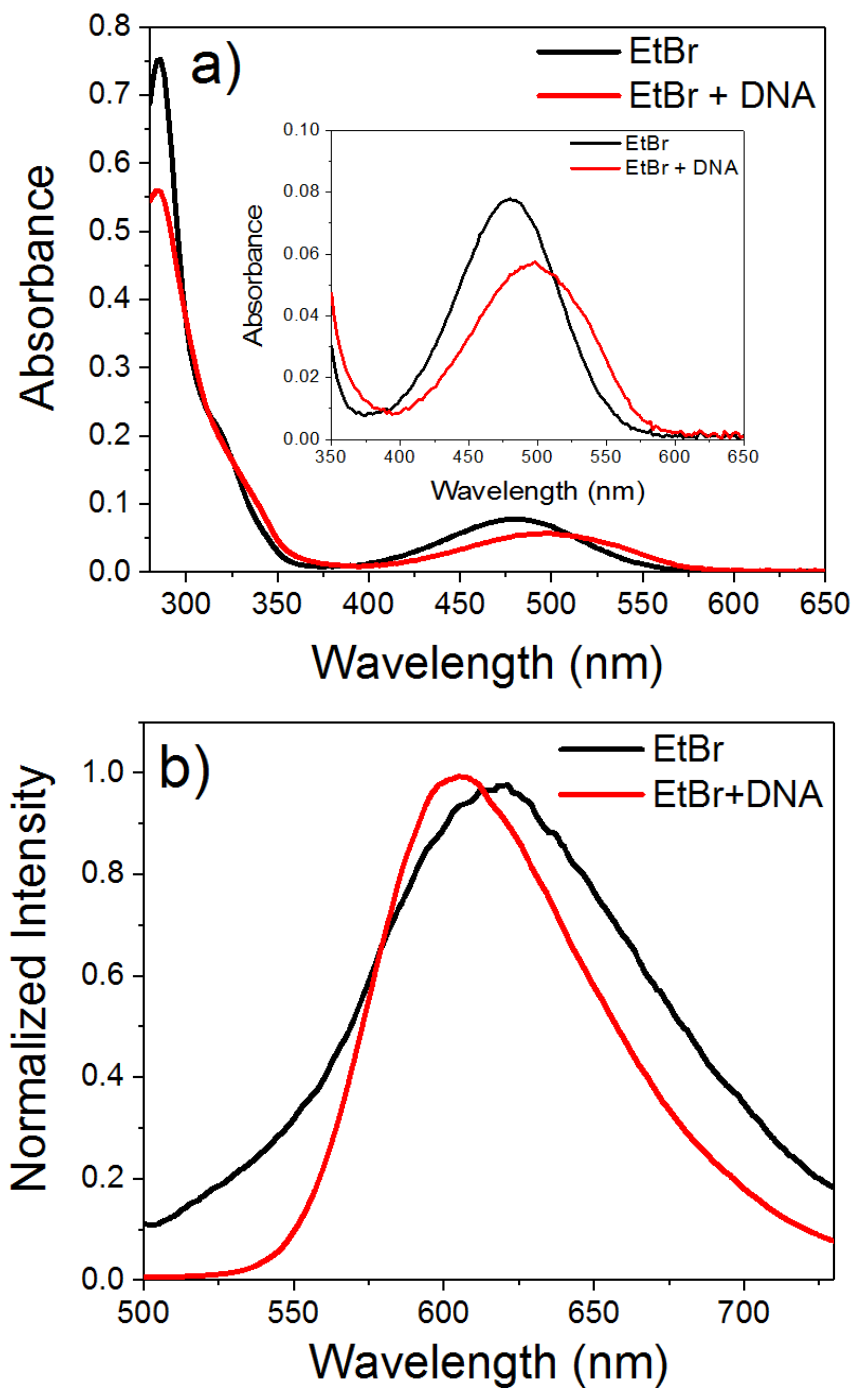


Figure 12: Absorption (a) and uncorrected normalized emission (b) spectra of free and DNA-bound EtBr.

In practical applications, to detect and visualize a small amount of DNA, typically, an excess of EtBr is used to ensure that all available DNA is exposed to the intercalator. Due to the relatively low affinity of EtBr to DNA, a significant excess of the dye is required, and the emission spectra from the free dye would end up dominating the signal. We cannot change/improve the binding affinity of EtBr to DNA, and the only option to enhance the detectability limit is to enhance the signal from EtBr bound to DNA.

Let us consider a DNA sample to which some amount of EtBr is added. The equilibrium between free and bound EtBr depends on the DNA and EtBr concentrations and the dissociation constant, k_d for binding. For the purpose of our simulation, we assume a single binding site for which the binding equilibrium will be given by (Kimball J D 2018), (Kitchner E 2021)

$$\theta_{EtBr} = \frac{(k_d + C_1 + C_2) - \sqrt{[(k_d + C_1 + C_2)^2 - 4C_1C_2]}}{2C_2}, \quad (7)$$

where θ_{EtBr} represents the fraction of bound probe (EtBr) to a target (DNA), and C_1 and C_2 are the concentrations of DNA and EtBr, respectively.

According to Equation (7), for a given amount of DNA, the fraction of EtBr bound to DNA will depend on the amount of added EtBr. The observed emission signal is the sum of the signals from the fraction of free and DNA-bound EtBr,

$$F = I_{ex} \cdot C_2 (\varepsilon_B \cdot QY_B \cdot \theta + \varepsilon_F \cdot QY_F \cdot (1 - \theta)), \quad (8)$$

where ε_F and ε_B are the extinction coefficients for free, and DNA-bound EtBr at the excitation wavelength, QY_F , and QY_B are the respective quantum yields, C_2 is the total concentration of EtBr, and I_{ex} is the excitation light intensity.

In Figure 13, the expected fluorescence signal measured as a function of EtBr concentration is presented for different DNA concentrations. For this simulation, a dissociation constant, $k_d = 10^{-5}$ M, was arbitrarily assumed, and the overall signal enhancement upon binding (due to the change in extinction coefficient and quantum yield) was assumed to be equal to 10. In the initial stages, the signal increases with a higher slope. For the low range of EtBr concentrations, the signal is dominated by the DNA-bound fraction of EtBr. When the EtBr concentration approaches the DNA concentration, the slope decreases and is driven by the increase of EtBr concentration (an increase of the free EtBr fraction). In real-world applications, the amounts of DNA are limited, and the amounts of EtBr are unknown. A relatively large amount of EtBr is used to ensure a sufficient signal, and the free EtBr fraction could significantly restrict the DNA detectability limit. Practical EtBr concentrations will typically result in more than half saturation of DNA. This should be within the end of the linear range of the initial part of the intensity increase in Figure 13.

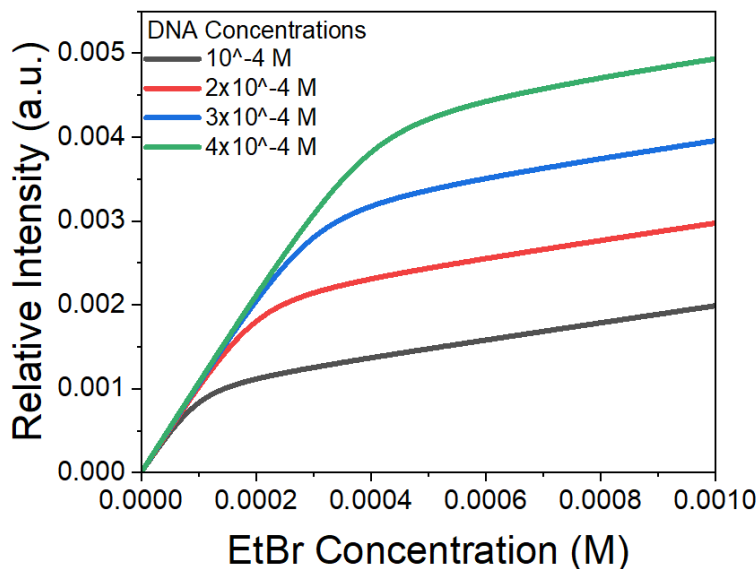


Figure 13: Expected fluorescence signal measured as a function of EtBr concentration for different concentrations of DNA.

CHAPTER 3: DETECTING DNA WITH MULTI-PULSING AND TIME-GATING APPROACH

As discussed in the *Theoretical Considerations*, when using a multi-pulsing approach for a lifetime much longer than the time separation between excitation pulses, the molecules in the excited state will not completely decay during the time between pulses, and each sequential pulse will add to the excited state population. Effectively, measurements starting after the last pulse in the burst will detect many more excited molecules with a longer fluorescence lifetime.

3.1: Selecting the pulse separation

Equation 6 (*Theoretical Considerations*) reports the number of excited molecules after n consecutive excitation pulses in the burst. Figure 14 shows the expected number of excited molecules (intensity is proportional to the number of excited molecules) for the long (22 ns) and short (1.6 ns) lifetime components as a function of the number of pulses in the burst.

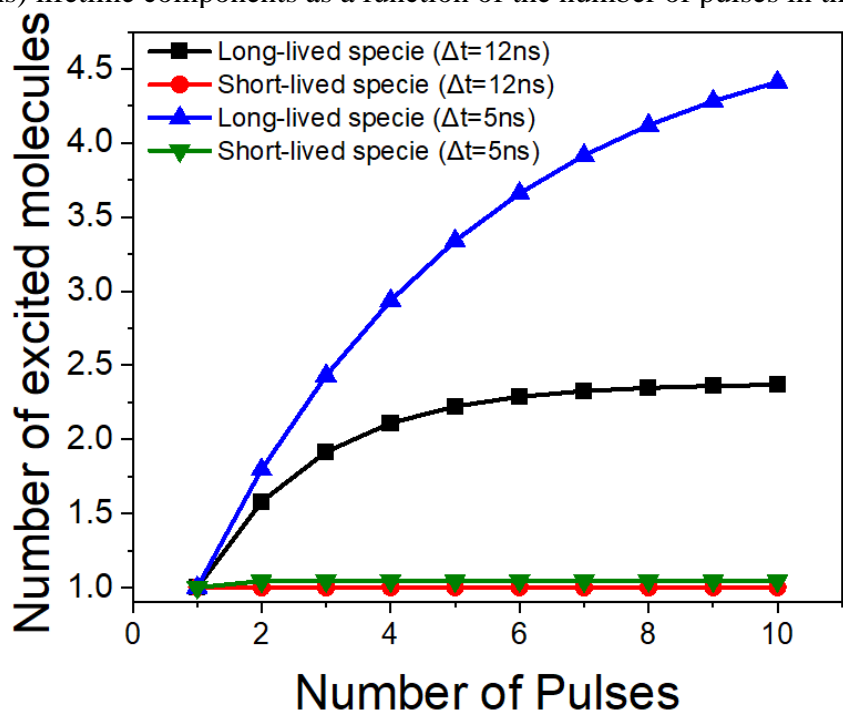


Figure 14: Expected number of excited molecules (intensities are proportional to the number of excited molecules) for the long (22 ns) and short (1.6 ns) lifetime components as a function of the number of pulses in the burst.

For the simulation reported in Figure 14, we considered the pulse separation in the burst to be 5 ns and 12 ns, respectively. The intensity of the long component quickly increases with the number of pulses. The increase is fast for the first few pulses and reaches the saturation level for more than 10. For a pulse-to-pulse separation in the burst $\Delta t = 5$ ns, the relative intensity observed for 4 pulses increases 3-fold for the long component and just 4% for the short component. Similarly, for a pulse-to-pulse separation in the burst $\Delta t = 12$ ns, the long-lived fraction increases more than 2-fold while the short-lived fraction practically does not change. Using pulse-to-pulse separation of about 5 ns would be beneficial, but this would require special designs, as discussed previously (Fudala R 2014), (Shumilov D. 2014). However, a pulse-to-pulse separation of 12.5 ns is easy to achieve with any laser diode for which the maximum repetition rate is 80 MHz. An electronic laser driver like our PDL 828 "Sepia II" (PicoQuant GbmH) can generate bursts of pulses where the pulse-to-pulse separation is 12.5 ns with any repetition rate for the bursts down to kHz.

Figure 15 presents the simulated spectra as expected from a system with 8% bound and 92% free EtBr fractions corresponding to a 50:50 intensity contribution of free (dashed black line) and bound (dashed red line). As anticipated, with 4-pulse excitation the long-lived fraction (solid red line) significantly increases and now contributes almost 3 times more to the total intensity (solid green line).

3.2: Selecting the time-gating

Next, time-gating was applied to the detection mode. As mentioned, time-gating is a passive approach and differently from pulsing, the initial signals will only decrease. Therefore, the sample must present a measurable signal for the lowest intensity fraction (the long-lived component in our case)

at zero time. The signal of the free fraction and bound fraction will decrease according to the delay time for the gate opening, as stated by Equation 3 (*Theoretical Considerations*). Therefore, for a short-lived fraction, the measured intensity will decrease much faster.

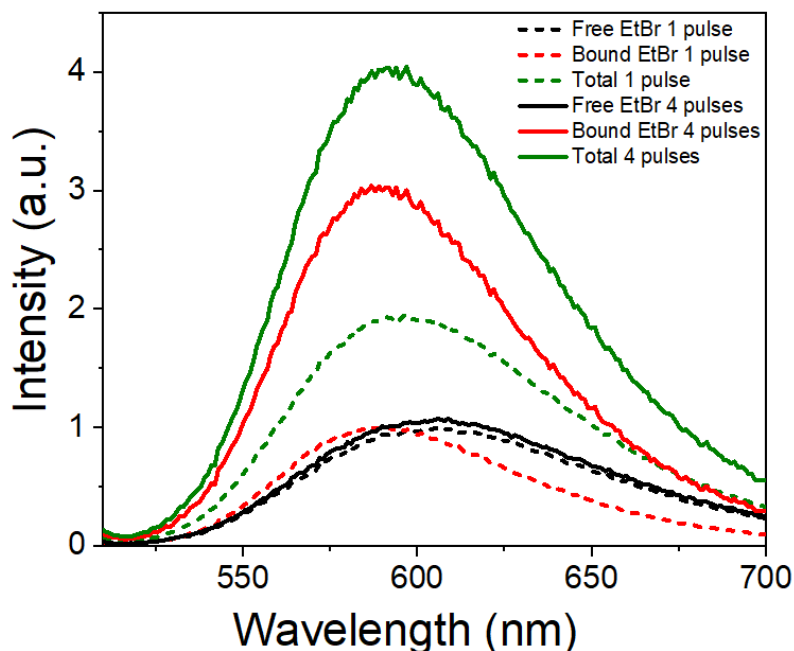


Figure 15: Simulated spectra as expected from the first system (8% bound and 92% free EtBr fractions corresponding to 50:50 intensity between free and bound at 485 nm excitation) single pulse excitation (dashed lines) and 4-pulse excitation (solid lines).

Figure 16 (panels A and B) presents the expected intensities from the free and bound EtBr fractions as a function of gate time opening. The top graph shows the simulated spectra as measured after a single pulse and without delay. Next, the expected relative intensities after 4 pulses are shown. The fraction of the long-lived component becomes three times greater. Following the panel, the expected spectra measured after 2 ns, 5 ns, and 10 ns delay time for gate opening with the 4-pulse excitation are shown. For panel A (2 ng/ μ l DNA concentration), the total signal is already dominated by the bound fraction after 5 ns. Moreover, after 10 ns, the intensity for the short-lived fraction is practically zero, while it drops only about 40% for the long-lived one.

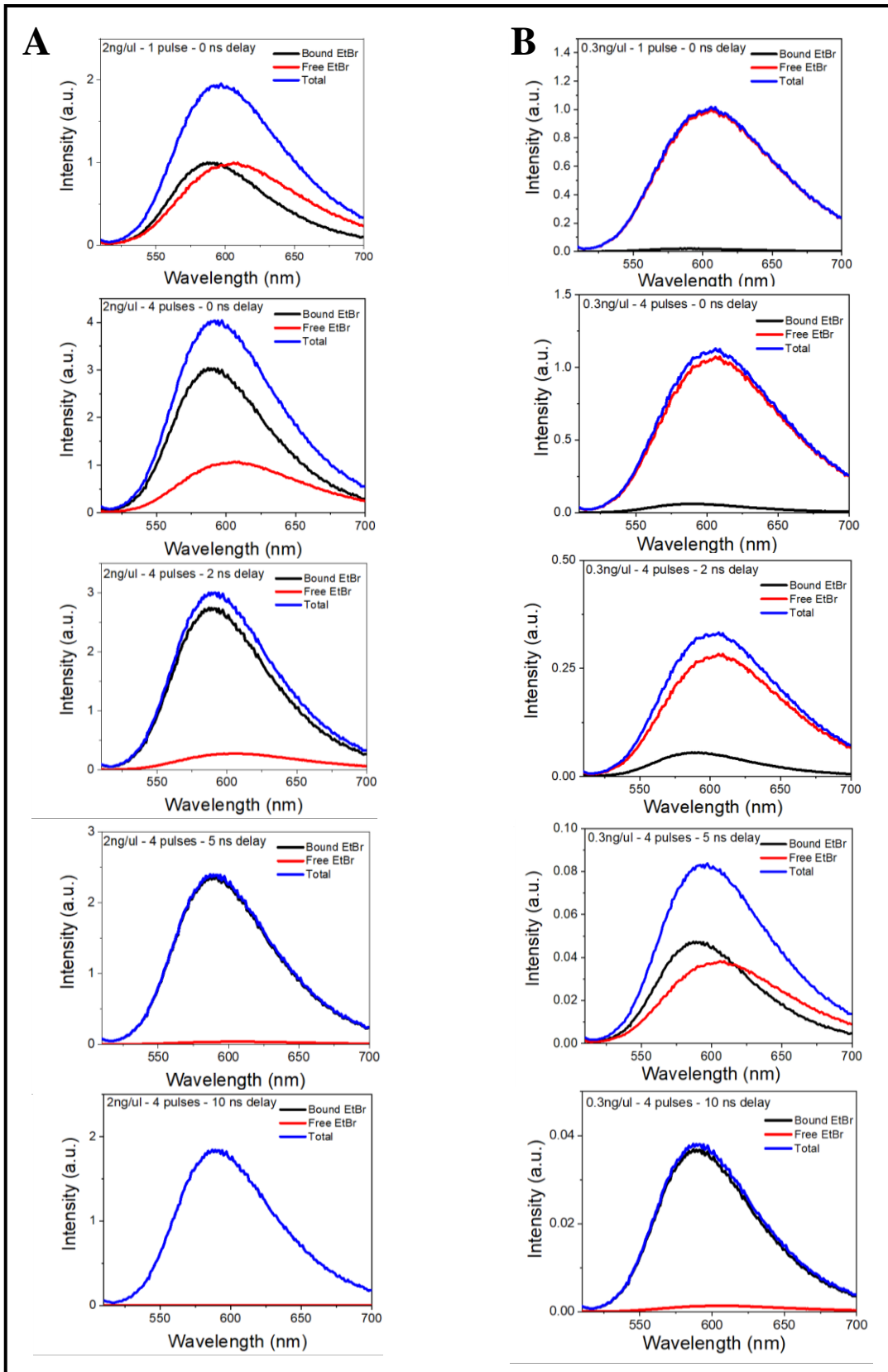


Figure 16: Expected emission intensities from the free and bound EtBr fractions as a function of gate time opening for two different concentrations of DNA: 2ng/μl (panel A) and 0.3 ng/μl (Panel B) after 4-pulse excitation burst. For comparison the top two graphs show intensities observed with single pulse excitation.

Similar behavior is observed for panel B (0.3 ng/ μ l DNA concentration). The bound fraction is expected to be below 0.2% and was practically impossible to detect with a single pulse. After 4 pulses, the trace of the long-lived fraction becomes a little more visible. The relative fraction of the long component increases with the delay time for gate opening, and after 10 ns, the signal from the bound form dominates the observed emission. It is evident that by measuring the intensity after a burst of 4 pulses or more with a gate delay time of 10 ns, the emission spectra well reproduce the fraction of EtBr bound to DNA.

Two important conclusions should be derived from these simulations. First, using a pulsed excitation mode, the signal of the desired fraction (EtBr bound to DNA) is increased almost three-fold for 4 pulses in the burst. Second, after more than 5 ns delay time in the gate opening, only the long-lived fraction (DNA bound EtBr) is detected. Consequently, since the intensity of the long-lived fraction (and total measured intensity) after more than 5 ns is the only signal detected, collecting an image (picture) under such conditions will exclusively reflect the bound form of EtBr, which in turn reveals the presence of DNA. At the same time, the intensity of the unwanted short-lived fraction is completely suppressed/eliminated (the short-lived fraction was not enhanced by pulsing, and it has been heavily suppressed by time-gating).

3.3: Experimental verification

We intend to experimentally demonstrate that photons detected after a 4-pulse excitation and 10 ns delay for gate opening exclusively come from EtBr bound to DNA.

3.3.1: Ethidium Bromide solutions

For such a demonstration, we prepared a stock solution containing a concentration of DNA equal to 100 ng/ μ l. This concentration was calculated from the measured absorption at 260 nm (equal to 2 in a 1 cm cuvette or 0.2 in a 1 mm cuvette). Subsequently, 0.21 ml of the DNA solution was

added to 9.79 ml of the EtBr solution, which resulted in a 2 ng/ μ l (50x dilution) DNA concentration in EtBr solution (an equivalent dilution of water-based EtBr solution 9.79 ml of EtBr solution +0.21 ml of water was also prepared). By mixing the EtBr solution containing DNA with the EtBr solution only, DNA solutions of 2 ng/ μ l, 0.6 ng/ μ l, 0.3 ng/ μ l, and 0.15 ng/ μ l concentrations were prepared (via subsequent dilutions).

3.3.2: Pulse generation

The fluorescence lifetime of EtBr bound to DNA is about 14 times longer than the fluorescence lifetime of free EtBr in solution. To increase the accuracy for detection of EtBr bound to DNA, we utilized bursts of pulses as described in the theoretical considerations paragraph. Previous studies described multiple ways for generating bursts of pulses (Shumilov D. 2014), (Rich RM. 2017). In order to generate multiple pulses in the burst, one can use a dedicated laser driver like the previously mentioned PDL 828 "Sepia II" (PicoQuant GbmH). However, even a simpler and more intuitive approach is possible. In fact, in principle one can manufacture a fiber composed of multiple fibers, each of which has a different length. For this specific practical application, a

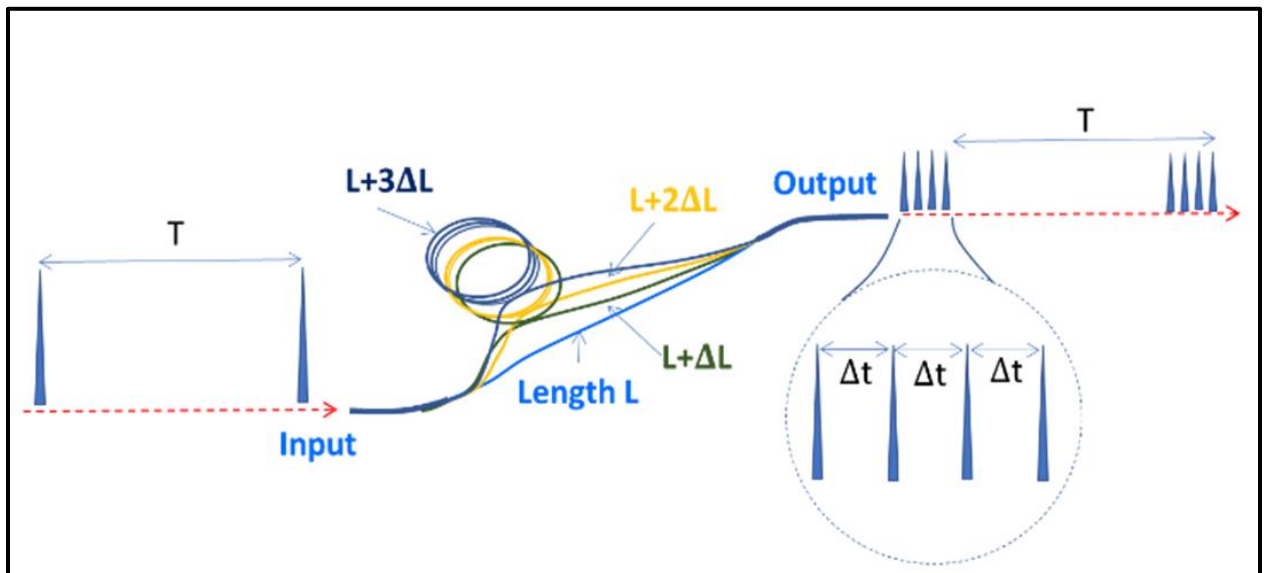


Figure 17: Schematic representation of the used fiber optics. The fiber splits into 4 equivalent branches, with the length of each branch increasing by about 75 cm.

custom-made fiber optics was made. Figure 17 shows a schematic representation of the utilized fiber optics.

The fiber splits into 4 equivalent branches, with the length of each branch increasing by about 75 cm. The excitation pulse is coupled to the fiber optics at one end, and as it goes through the fiber, it splits into 4 different branches that, at the end, come together to a single output. As a result, each pulse travels a different optical path, and at the output the 4 pulses are separated by about 4 ns between each other. A burst of 4 pulses separated by about 4 ns would greatly increase the detected fraction of DNA-bound EtBr without any meaningful change in the observed fraction of free EtBr. Figure 18A shows a burst of 4 pulses as measured with a scatterer (i.e., Ludox) using a Time Correlated Single Photon Counting (TCSPC) system from Horiba Scientific (DeltaFlex). Figure 18B illustrates the decay obtained with a burst of 4 pulses with a solution of EtBr without DNA, and Figure 18C shows a burst from a solution of EtBr saturated with DNA (about 95 ng/ul concentration). The intensities of each pulse in the burst are almost identical. It is rather difficult to couple the light to the fiber so that the intensity of each pulse in the burst will be identical. In practice, the intensity between pulses in the burst varies slightly. The first pulse is about 30% stronger (Figure 18A), but it does not change during the experiment, and the bursts are identical over time. The fluorescence intensity between pulses as measured from free EtBr solution (1.6 ns fluorescence lifetime) does not change from pulse to pulse, and fluorescence intensity practically decays after each pulse (Figure 18B). However, for DNA-bound EtBr (20 ns fluorescence lifetime), the intensity increases from pulse to pulse, and after 4 pulses, it is 3 times higher than the initial intensity after 1 pulse. Starting photon collection after the 4th pulse (triggering a detector with a delay) enhances the signal of the long component (DNA-bound EtBr) in relation to the signal from free EtBr, which significantly increases the sensitivity for detecting the long-lived fraction. To further increase the relative contribution of the long-lived fraction, the time-gated

detection approach can be used to start the measurement after a fixed time delay following the last excitation pulse.

3.3.3: Results

In Figure 19, time-resolved emission spectra (TRES) are presented as measured with 4 pulse excitation bursts after a time delay of 0 ns, 2 ns, 5 ns, and 10 ns after the last pulse in the burst for

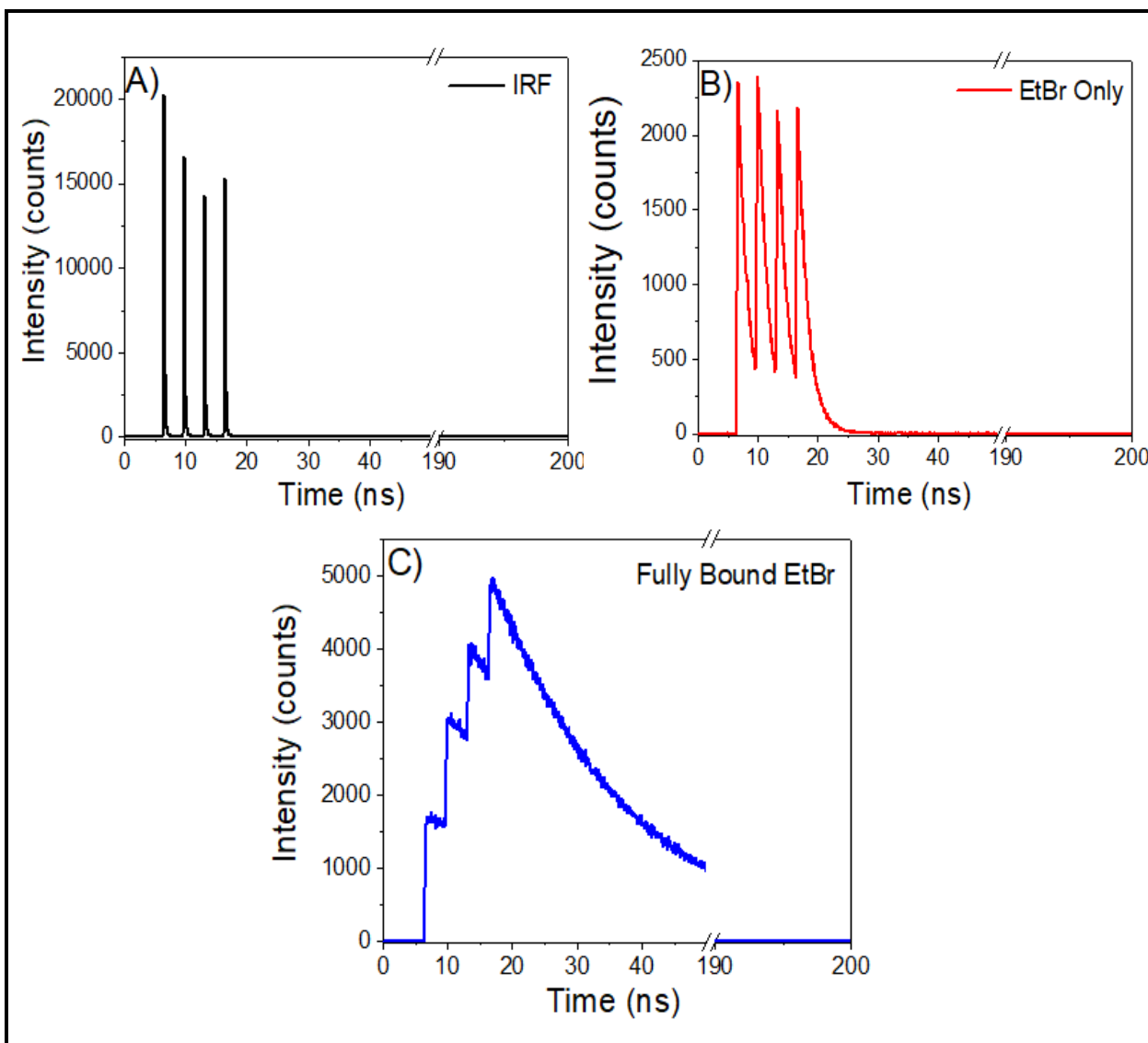


Figure 18: Burst of 4 pulses as measured in time correlated single photon counting (TCSPC) system (DeltaFlex from Horiba Inc.): Ludox scattering (0 fluorescence lifetime) (A), Emission of free EtBr solution (1.5 ns fluorescence lifetime) (B), and Emission from a solution of EtBr that is saturated with DNA (~ 95 ng/ μ l) (C).

three DNA concentrations (the concentration of EtBr is kept constant for each DNA concentration). In the first column of Figure 19, the highest concentration of DNA (2 ng/ μ l) is reported. Such concentration corresponds to about 3% of EtBr bound to DNA (97% of free EtBr in solution). When applying a 4-pulse burst excitation, the intensity fraction increases after each pulse, and after the 4th pulse, the long-lived fraction constitutes about 75% of the total intensity at 0 time. As the time delay increases, the short-lived fraction quickly decays. After a 10 ns delay, the signal of the long component completely dominates (only the signal from the long component can be detected). For a lower concentration of 0.6 ng/ μ l (middle column in Figure 19), the bound fraction is less than 1%, and the apparent initial fraction of the long-lived component after the 4th pulse in the burst is slightly more than 17%. The relative fraction of the long component (EtBr bound to DNA) increases quickly for increasing delay for gate opening. After 10 ns, the intensity fraction of the bound component is over 95%. The same is observed for the even lower concentration of 0.3 ng/ μ l (right column in Figure 19). The overall signal is obviously lesser for lower DNA concentration, but after 10 ns, only the long-lived fraction (EtBr bound to DNA) is visible. It is important to notice that in all cases, the intensity fraction of the long-lived component between 0 ns time delay and 10 ns time delay drops less than 50%, while the intensity of the short-lived component falls almost to zero (over 99.5%). Therefore, even starting with a dominant fraction of short-lived component (over 99%), the detected signal after 4-pulse excitation and delay of 10 ns or longer would only be due to the bound fraction. This approach provides a highly sensitive method to detect trace amounts of DNA present in the sample using a relatively high EtBr concentration.

Finally, to demonstrate the possibility of applying pulsed excitation and time-gated detection to expose/visualize and detect small amounts of DNA present in a sample, two solutions of low DNA concentrations (0.3 ng/ μ l and 0.15 ng/ μ l) were prepared and tested. Three small wells were drilled

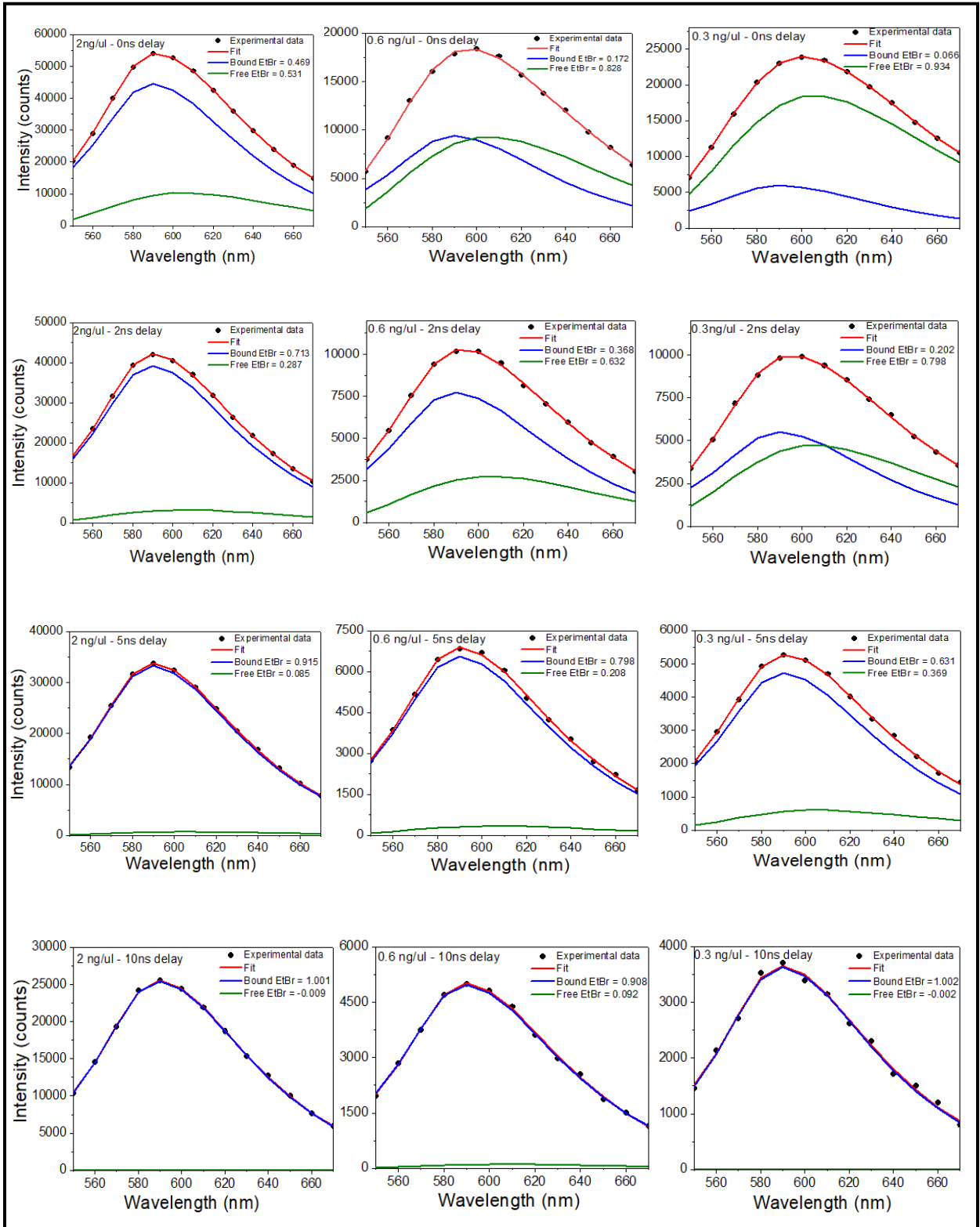


Figure 19: Time Resolved Emission Spectra (TRES) as measured with 4 pulses excitation burst after a time delay of 0 ns, 2 ns, 5 ns, and 10 ns after the last pulse in the burst, respectively for three DNA concentrations 2, 0.6 and 0.3 ng/ul (the concentration of EtBr is kept constant for each DNA concentration).

on a Teflon cuvette cap, as illustrated in the picture in Figure 20. Each well can be filled with about 2–3 μl of solution. The wells were filled with about 2.5 μl of a free EtBr solution, a solution containing EtBr and DNA, and a buffer (as reference), as marked in Figure 20 (top). An amount of about 2.5 μl of the DNA/EtBr solution of 0.3 $\text{ng}/\mu\text{l}$ contains about 750 pg of DNA (higher concentration), and when filled with the lower concentration solution (0.15 $\text{ng}/\mu\text{l}$), about 375 pg of DNA. A 485 nm excitation laser diode was used through a fiber that produces 4-pulse bursts, as presented in Figure 17. The repetition rate for the laser diode on the excitation was 1 MHz (the highest repetition rate accepted by our camera), leading to 4-pulse bursts separated by 1000 ns.

The photograph reported in the top left corner of Figure 20 shows the experimental setup with the three wells illuminated with the excitation beam. On the left side of the photograph, a dime is positioned for size reference. In order to image the wells, a 5x objective was used. On the top right side, the image field is shown as seen by the camera (the imaging camera took a photograph with ambient light excitation), where the wells are clearly visible. The camera must be synchronized with the pulsed laser diode, and a 40 ns gate (time for which the detector remains open) was set to ensure that most photons emitted by EtBr with long (20 ns) lifetime are collected.

The camera has the ability to adjust the gate time with a resolution of 0.5 ns. Since the physical gate cannot be instantaneously opened and the rise time is in the order of nanoseconds, even a short-lived (1.5 ns) decay will be spread over time. In order to prevent the excitation light from reaching the CCD detector of the camera, a 535 nm long pass filter was used. In the lower part of Figure 20, the images collected for different delays in gate opening time are shown. The first reported delay is 0 ns (no delay). After such time, the image intensity decreases as the delay time increases.

The top row of images shows EtBr only (in the left well) and EtBr with ~ 750 pg of DNA (in the right well). The lower well filled with buffer is invisible, showing that background is completely

eliminated (suppressed). At time 0 ns, the image of the DNA well is slightly brighter due to a small amount of DNA-bound fraction. As the gate opening time is delayed (keeping the gate width of 40 ns constant), the brightness of the left well (EtBr only well) quickly disappears, and for delays longer than 15 ns, the left well is entirely invisible. Contrastingly, the brightness of the right well-containing DNA drops only 50%.

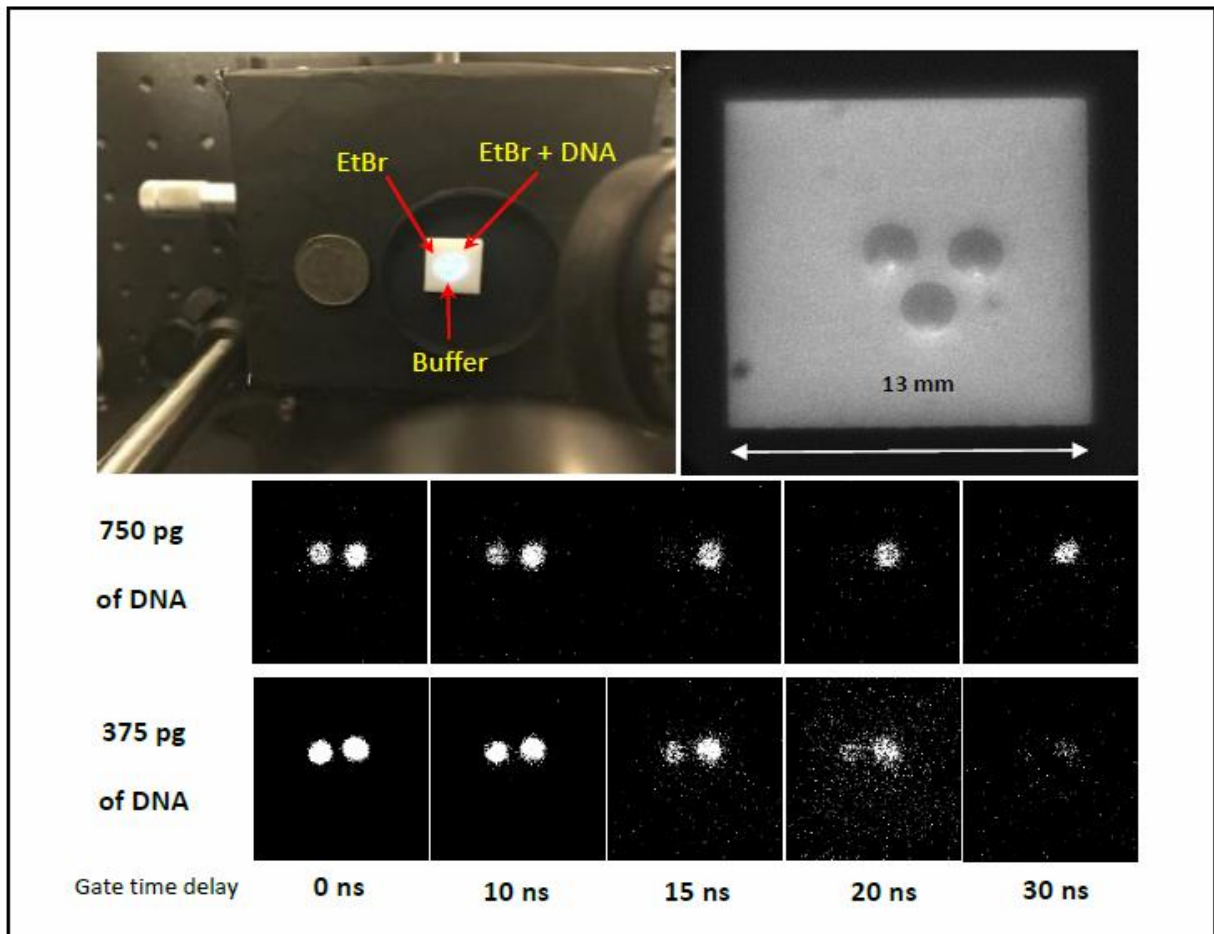


Figure 20: Time-delayed images of three wells filled with buffer, EtBr solution, and EtBr solutions with different amounts of DNA. Top left – photography of imaging stage with Teflon cuvette cap with three drilled small wells in the center. Top right – camera image of the cap acquired with the 5X objective utilized for the experiment. Bottom – images collected for different delays of gate opening time for two different amounts of DNA in the right well.

Similar behavior is shown by the lower row of images, where only 375 pg of DNA are present. The initial brightness (0 ns time) for EtBr only and EtBr with DNA is practically equal. However,

by increasing the time delay, the left well disappears much faster. Since the image intensifier gain and the number of collected frames to detect images need to be increased, the free EtBr is visible longer. However, collecting each image still takes less than 5 s. Importantly, even with increased sensitivity, the well with buffer (background) is not visible.

3.4 Summary

In conclusion, applying a technique based on multi-pulse pumping and time-gated detection, we successfully detected the presence of an amount of DNA as low as about 300 pg/ μ l.

However, since the reference background signal from the well filled with buffer is completely undetectable at the used conditions, the detection sensitivity could be potentially significantly increased by using a higher power excitation laser diode and/or by utilizing a laser diode with an excitation wavelength of 540 nm or even 560 nm that preferentially excites EtBr bound to DNA. In addition, by applying this technology to dyes that may exhibit higher affinity to DNA (e.g., DAPI, YOYO, or DiamondTM), detection sensitivity can be efficiently increased by at least an order of magnitude.

CHAPTER 4: USING FORSTER RESONANCE ENERGY TRANSFER TO ENHANCE SENSITIVITY AND SPECIFICITY FOR DNA DETECTION

Recently, we realized that Foster Resonance Energy Transfer (FRET) between intercalating dyes could be used to further increase the detection sensitivity and specificity of trace amounts of DNA in a sample. FRET is a radiationless energy transfer process from an excited chromophore (called a donor) to a chromophore that presents suitable spectral properties called an acceptor.

The energy transfer is a "through space" interaction and can happen between two chromophores that have suitable spectral properties and are separated by a distance below 100 Å. Because of this reason, FRET is rarely observed for free dyes in solution since the required concentration of

acceptor is very high (i.e., mM to M range). However, DNA can provide a scaffold where two intercalated dyes can be immobilized in close proximity even if the concentrations of the dyes are low.

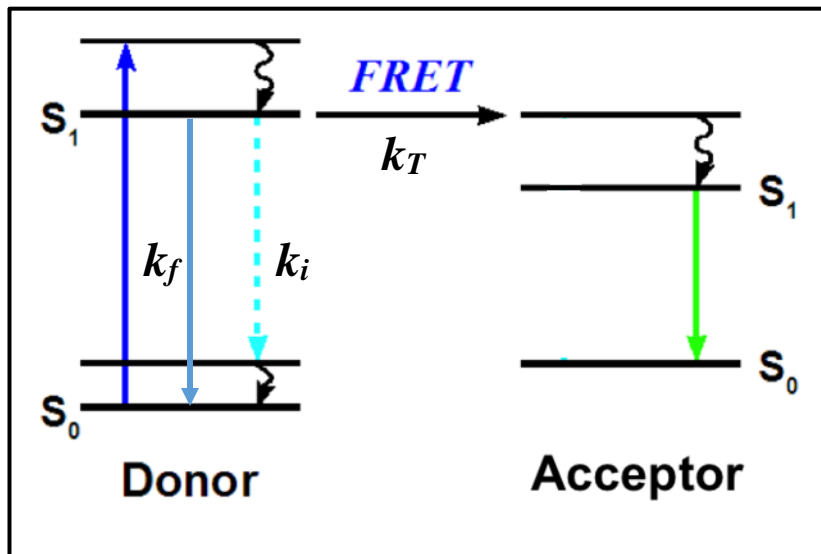


Figure 21: Jablonski diagram of electronic states for donor and acceptor, showing the process of FRET.

4.1: Theory

Figure 21 shows the Jablonski diagram of electronic states for donor and acceptor.

The efficiency of FRET can be described by

$$E = \frac{k_T}{k_f + k_T + \sum_i k_i}, \quad (9)$$

where k_T , is the energy transfer rate, k_f is the radiative decay rate of the donor and k_i indicates all the other possible decay rates of the donor. The theory for resonance energy transfer (RET) is rather complex, and we will discuss only the final results. For a very weak coupling, where the energy of interaction between donor and acceptor is small compared to the vibrational splitting of the donor energy levels, the classical and quantum mechanical approaches yield essentially an identical dependence. Considering a single donor and acceptor separated by a distance r , one can calculate the rate of transfer (probability of transfer of energy from donor to acceptor per unit

time),

$$k_T = \frac{Q_D \kappa^2}{\tau_D r^6} \left(\frac{9000 \ln 10}{128 \pi N n^4} \right) \int_0^\infty F_D(\lambda) \varepsilon(\lambda) \lambda^4 d\lambda, \quad (10)$$

where Q_D is the quantum yield of the donor in the absence of the acceptor; τ_D is the lifetime of the donor in the absence of the acceptor; n is the refractive index of the medium; N is Avogadro's number; F_D is the normalized fluorescence intensity of the donor (area under the curve normalized to unity); $\varepsilon(\lambda)$ is the extinction coefficient of the acceptor at λ ; κ^2 is the orientational factor describing the relative orientation in the space of the transition moment of donor and acceptor. The integral in Equation (10), referred to as overlap integral $J(\lambda)$, expresses the extent of spectral overlap between the donor emission and acceptor absorption and is given by,

$$J(\lambda) = \frac{\int_0^\infty F_D(\lambda) \varepsilon(\lambda) \lambda^4 d\lambda}{\int_0^\infty F_D(\lambda) d\lambda}. \quad (11)$$

$F_D(\lambda)$ is dimensionless. If the extinction coefficient $\varepsilon(\lambda)$ is expressed in units of $M^{-1}cm^{-1}$ and λ in nanometers, then $J(\lambda)$ is in units of $M^{-1}cm^{-1}nm^4$. We can then express the rate of transfer reported in Equation (10) as

$$k_T = \frac{1}{\tau} \left(\frac{R_0}{r} \right)^6, \quad (12)$$

where the term R_0 is equal to $8.79 * 10^3 [Q_D \kappa^2 n^{-4} J(\lambda)]^{1/6}$. The term R_0 is the characteristic Forster distance, and its meaning can be understood from the frequently used form of Equation (10). In practice, R_0 represents the donor-acceptor separation for which 50% of the excitation energy will be transferred to the acceptor (in reality, 50% of the excited donors will transfer the excitation energy to the acceptors). It is important to realize that the energy transfer process competes with the spontaneous decay of the donor, which proceeds with the rate constant $k_f +$

$\sum_i k_i$.

According to Equation (10), in order for FRET to happen, two fluorophores (donor and acceptor) should present a significant spectral overlap. In other words, the acceptor needs to absorb where the donor emits. More specifically, the energy of the emission radiation of the donor needs to match the energy gap between the relaxed/ground and excited state of the acceptor. However, the FRET process happens without the emission of a photon by the donor. The transfer efficiency, E , can now be expressed as a function of the donor-acceptor separation and the characteristic Forster distance, R_0 ,

$$E = \frac{1}{1 + \left(r/R_0\right)^6}. \quad (13)$$

The sixth power of the distance r between the chromophores causes a very rapid decrease in the possibility for FRET to happen when the distance is slightly bigger than R_0 . The absorption of EtBr extends up to 600 nm, and it could be a good acceptor for any emitters in the range below 600 nm.

In the following part of this thesis, we will discuss the possibility of merging the use of dyes with high affinity to DNA (e.g., DAPI or YOYO) and EtBr. Through this we can still take advantage of the long-lived decay of bound EtBr, but we can also increase the sensitivity and specificity for detection thanks to the interaction between the dyes via Forster Resonance Energy Transfer (FRET), which happens exclusively in the presence of DNA.

4.2: How FRET can be useful for DNA detection

One of the disadvantages of EtBr is the low extinction coefficient in the visible range. This is the reason why most practical applications using EtBr utilize ultraviolet (UV) excitation (290 nm),

which is unsuitable for use with cells, tissue, or any biological substrate. YOYO, in contrast, has a much over 10 times higher extinction coefficient at 480 nm range than EtBr itself. There are three main reasons for utilizing FRET for DNA detection:

- (1) The much higher extinction coefficient of YOYO in the visible range. Furthermore, the emission of YOYO is below 600 nm, making it a suitable candidate as an energy donor to EtBr. An efficient FRET will highly enhance the overall signal observed from EtBr.
- (2) The emission of EtBr is above 600 nm range, and the contributions of autofluorescence of biological components and the majority of substrates are much lower. This will enable simple imaging and DNA visualization.
- (3) In order to observe FRET, both the donor and acceptor must be immobilized within the same DNA strand. This enormously increases the specificity for DNA detection.

Now, let us consider a solution of DNA and EtBr to which another intercalator (YOYO) with higher binding affinity to DNA is added. At the initial stages, YOYO will bind to the free binding sites, but YOYO will also compete for binding with EtBr, consequently replacing EtBr. In general, YOYO (or any other intercalator) may have multiple binding sites, not necessarily the same as the binding sites for EtBr. As a first approximation, DNA is a simple linear system (1D symmetry) (Matveeva EG 2010), (Murata SI 2000), and bound YOYO will have a high probability of being close to DNA-bound EtBr. In Figure 22, we schematically represent a double-stranded DNA with YOYO and EtBr intercalated. Additionally, we included the approximate DNA dimensions (width of 20 Å) and the size of a full turn for the DNA helix, measuring about 35 Å. A rough estimation of R_0 for the YOYO – EtBr system when bound to DNA yields a Forster distance for these two dyes in the range of 40 Å (importantly, when free in solution, the quantum yield of the donor (YOYO) is very low, its fluorescence lifetime is very short, and R_0 is below 30 Å, strongly limiting the interaction of free dyes in the solution).

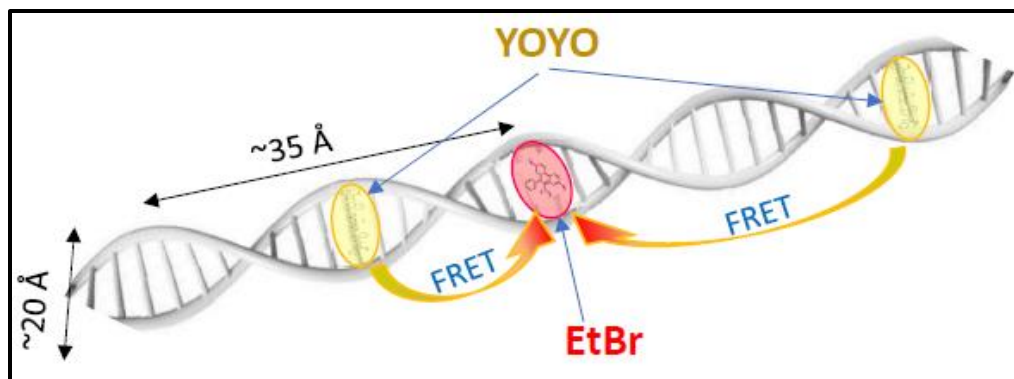


Figure 22: Schematic of the DNA with EtBr and YOYO intercalated. In the figure we included the approximate dimensions for the DNA helix.

The R_0 , when bound to DNA, is significantly larger than the potential separation between YOYO and EtBr intercalated to the same strand of DNA. Since the DNA scaffold is linear, there is a good probability that the YOYO binding sites will be within a few nm from at least one EtBr bound to DNA, which would be in the Forster resonance energy transfer (FRET) range allowing for highly efficient excitation energy transfer. If so, a significant excitation energy transfer from YOYO to EtBr would be expected. Efficient energy transfer will highly enhance the fluorescence signal observed from EtBr. Also, as YOYO concentration is increased, YOYO will begin to replace EtBr bound to DNA, forcing EtBr to the solution (the free unbound EtBr fraction will be increasing). A precise solution to this problem would require exact knowledge of the multiple binding sites, the dissociation constants, and the respective concentrations. In our experiments, dye/intercalator concentrations can be controlled. However, for typical applications just aiming to detect the presence of DNA (e.g., forensic applications), one cannot predict the amount of DNA present in a particular case/target site. So, only qualitative questions can be addressed about what signal behavior can be expected in an experiment in which there is a fixed amount of DNA to which a certain amount of EtBr is added and then followed with consequential additions of YOYO. We

discuss the simplest case of one binding site to qualitatively understand if such an approach could be beneficial.

Let us consider a solution of DNA with a given concentration to which a known concentration of EtBr is being added. The equilibrium is described by Equation (7), and the observed fluorescence of EtBr (total signal from bound and free EtBr) is described by Equation (14). For simplicity, we assume that DNA has only one type of binding site for both EtBr and YOYO. To further simplify the competitive binding problem and obtain a simple and qualitative solution, we assume that the binding affinity of YOYO is at least an order of magnitude higher than the binding affinity of EtBr. In this case, applying Equation (7), the binding equilibrium for YOYO and the fraction of EtBr bound to DNA can be calculated as a function of YOYO concentration for a fixed amount of DNA and a fixed amount of EtBr. These assumptions allow for the total signal observed from EtBr to be calculated as a function of YOYO concentration described as follows:

$$F_{EtBr}(C_{YOYO}) = I_{ex} \cdot C_{EtBr} \cdot (\theta_{EtBr}^{YOYO} \cdot \varepsilon_B \cdot QY_B + (1 - \theta_{EtBr}^{YOYO}) \cdot \varepsilon_F \cdot QY_F) + I_{ex} \cdot C_{YOYO} \cdot \varepsilon_{YOYO} \cdot \theta_{YOYO} \cdot EF \cdot QY_{YOYO}, \quad (14)$$

where C_{YOYO} is the concentration of YOYO, θ_{YOYO} represents the fraction of YOYO bound to DNA, QY_{YOYO} is the quantum yield of YOYO bound to DNA, ε_{YOYO} is the extinction coefficient of YOYO at the excitation wavelength, EF is the FRET efficiency, and θ_{EtBr}^{YOYO} is the fractional saturation of EtBr at a given YOYO concentration. If the extinction coefficient of YOYO is higher than EtBr and there is high efficiency for energy transfer from YOYO to EtBr, the addition of YOYO should result in a fluorescence signal increase.

In order to graphically demonstrate the expected behavior, we assumed a concentration of $10^{-4}M$ for EtBr, a dissociation constant of $10^{-5}M$ for EtBr and $10^{-6}M$ for YOYO. We also assumed that the extinction coefficient for YOYO is 10 times greater than for EtBr, and the energy transfer

efficiency is 80%. The simulated plots reporting the EtBr relative intensity versus YOYO concentration for different DNA and EtBr concentrations are indicated in Figure 23. As the concentration of YOYO increases, the relative intensity of EtBr initially increases due to the energy transfer. After a plateau, the relative intensity of EtBr decreases because YOYO displaces EtBr, and forces it outside of DNA, thus increasing the amount of free fraction of EtBr (lower QY).

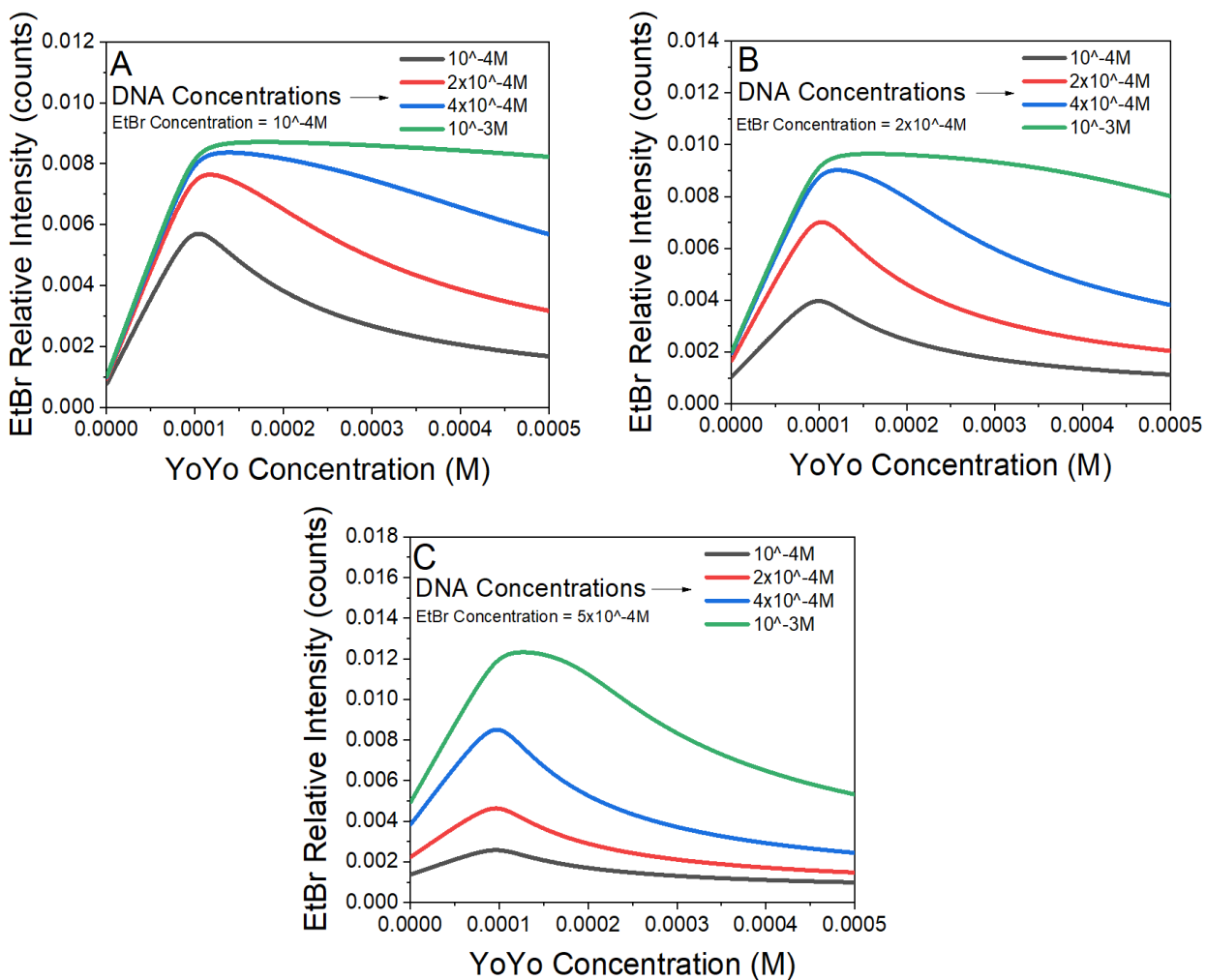


Figure 23: Expected fluorescence signal measured as a function of YOYO concentration for different concentrations of DNA and EtBr. The concentration of EtBr was varied from $10^{-4} M$ (A) to $2 \times 10^{-4} M$ (B) and to $5 \times 10^{-4} M$ (C).

4.3: Experimental results

Figure 24 presents the absorption spectra of YOYO and EtBr in phosphate-buffered saline (PBS) without DNA and with DNA. We used an arbitrary concentration of dyes that allowed us to obtain comparable absorptions to represent the effect qualitatively. Both dyes can be sufficiently excited with a light in the 450-500 nm range where good laser diodes are readily available. However, the extinction coefficient of YOYO in the visible range (450-500 nm) is much higher than the extinction coefficient of EtBr, and the concentration of YOYO used is much lower than the concentration of EtBr.

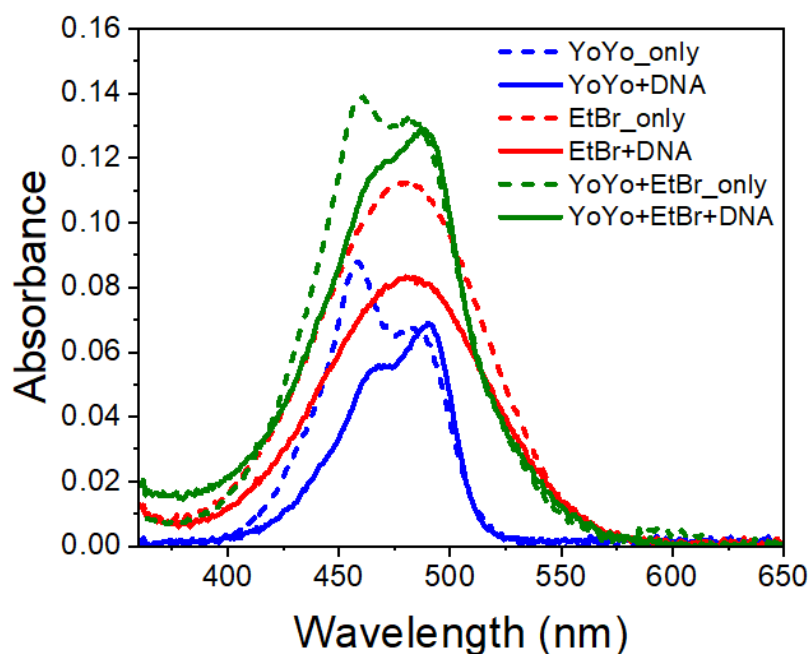


Figure 24: Absorption spectra of intercalators YOYO and EtBr in phosphate buffered saline (PBS), free and bound to DNA. The concentrations of the dyes are arbitrary to achieve a comparable absorption range.

Figure 25 shows uncorrected emission spectra of YOYO and EtBr in PBS without DNA and with a small amount of DNA added (an amount of DNA that is insufficient to saturate EtBr), measured with a 485 nm excitation laser diode. The emission spectra with a limited amount of added DNA revealed different affinities for binding to DNA. In fact, the emission spectra are normalized to the signal observed with the DNA, and the emission spectra of the free dyes (before DNA addition)

are drawn into the scale (dashed lines). When DNA is added to the sample, the emission of YOYO increases significantly, presenting a sharp maximum at about 510 nm. On the other hand, the emission of EtBr upon binding to DNA increases only moderately (for the used excitation, about a 4-5-fold increase is expected when saturated with DNA (Kitchner E 2021), and the emission is shifted toward the blue with a maximum emission at about 610 nm.

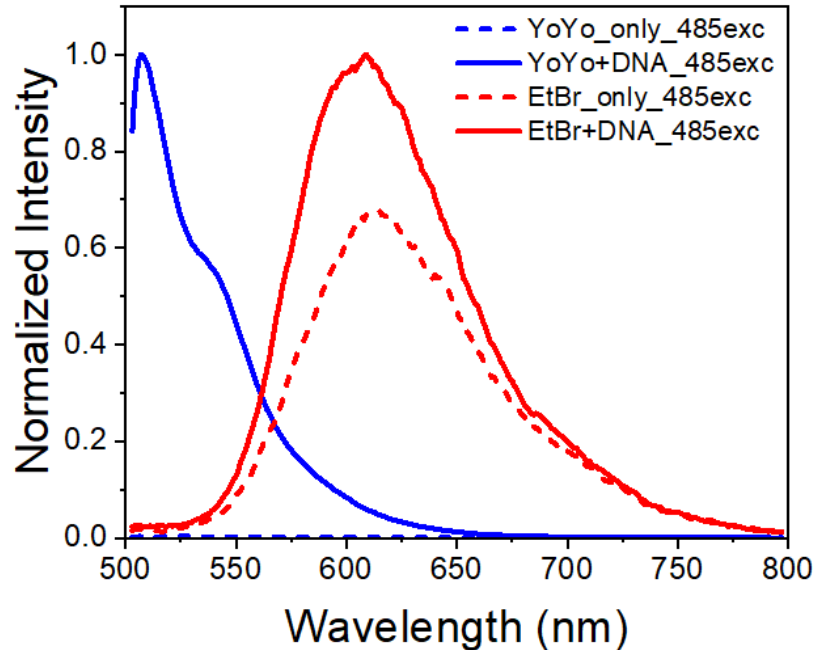


Figure 25: Uncorrected emission spectra of YOYO and EtBr in phosphate buffered saline (PBS) without DNA and with DNA observed with a 485 nm excitation diode. The emission spectra are normalized to the signal observed with the DNA.

As we showed for DAPI (Ceresa L. 2021), obtaining excitation spectra for a mixture of EtBr and YOYO is a very useful tool to demonstrate the actual occurrence of FRET. Therefore, in Figures 26 A and B, we present excitation spectra for YOYO and EtBr as free dyes in solution and dyes in solutions to which DNA was added, measured for two observation wavelengths, 520 nm, and 620 nm, respectively. The excitation spectrum of YOYO observed at 520 nm has a maximum peak at about 490 nm, and the excitation spectrum of EtBr is practically negligible (there is no emission of EtBr at 520 nm). On the other hand, for the observation wavelength, 620 nm, the distinct

excitation spectrum of EtBr is detected. The same observation wavelength for YOYO only shows a minimal trace of the YOYO excitation spectrum (at 620 nm, the emission of YOYO is much weaker than the YOYO emission observed at 520 nm). The excitation spectrum for a mixture of the two intercalators without DNA closely resembles the sum of the measured spectra for YOYO

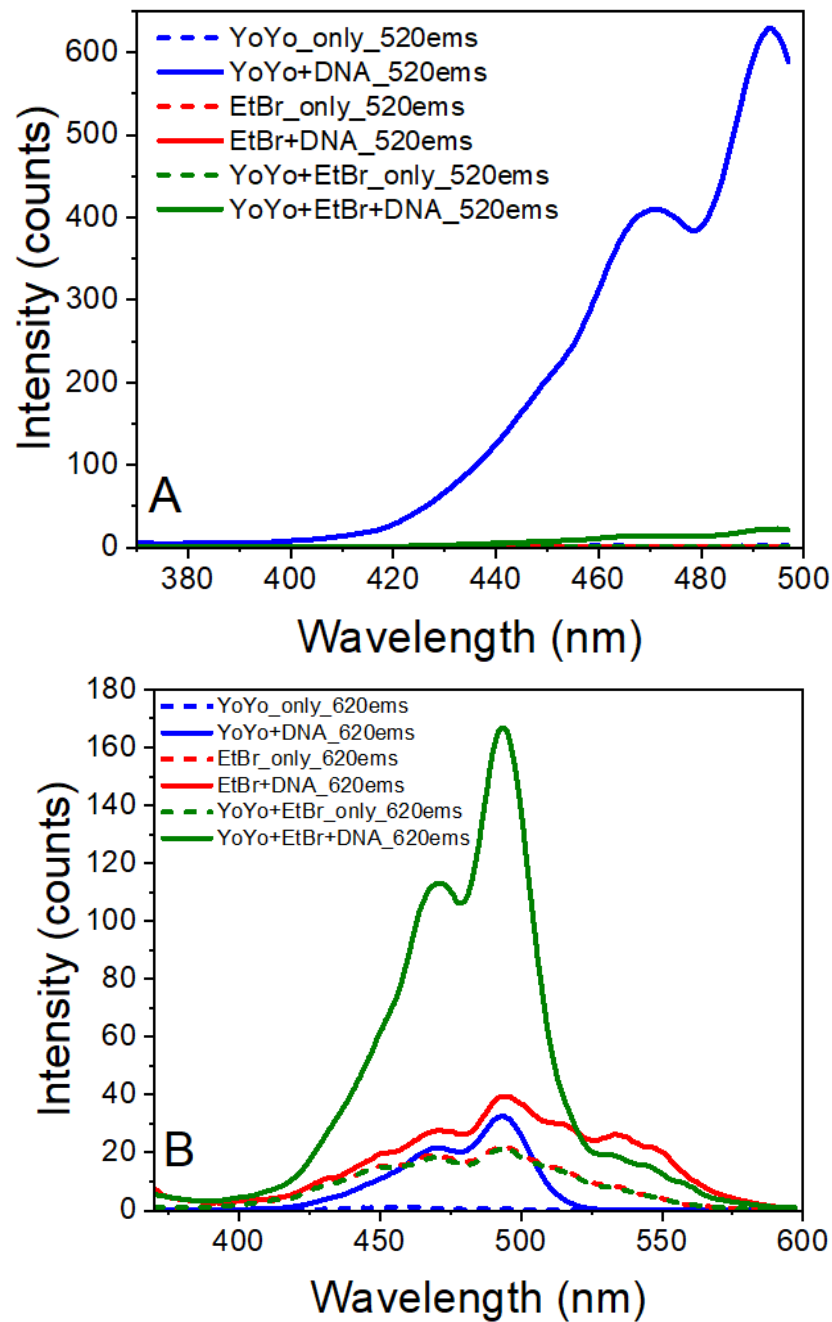


Figure 26: Excitation spectra of YOYO and EtBr as single dyes and mixed, with and without DNA, measured at 520 nm emission (A) and 620 nm emission (B).

and EtBr independently. Good spectral additivity indicates that these two dyes do not interact in solution significantly at the used concentrations (without DNA added).

In contrast, the excitation spectra of the same mixture with added DNA show dramatic differences. For 520 nm observation, the excitation spectrum is much smaller than the corresponding spectrum of just YOYO with DNA (quenching of YOYO) (Figure 26A). The difference is even more dramatic for 620 nm observation. The excitation spectrum measured at longer wavelengths (above 525 nm) reproduces the spectrum obtained from a solution of EtBr with DNA well. However, at shorter wavelengths below 520 nm, a clear contribution from YOYO absorption is evident. At about 490 nm (maximum of YOYO absorption), the excitation spectrum is almost 4 times stronger than for EtBr alone. These two facts (quenched emission of YOYO in the mix at 520 nm observation and clear contribution of YOYO at 620 nm observation (acceptor emission wavelength)) indicate significant excitation energy transfer.

To further demonstrate the radiationless mechanism of excitation energy transfer from YOYO to EtBr, we measured the emission spectra of EtBr saturated with DNA with increasing concentrations of YOYO. Specifically, we did so by using two excitation wavelengths; 535 nm excites EtBr bound to DNA well and doesn't excite YOYO, and 485 nm excites both dyes. For this experiment, a DNA concentration of 5 ng/ μ l was used. The results are reported in Figures 27 A and B. For 535 nm excitation, the intensity of the EtBr signal decreases as we increase the concentration of YOYO (Figure 27A). Contrarily, we observed an increase in the EtBr signal excited at 485 nm upon the addition of subsequent amounts of YOYO (Figure 27B). Starting with 10 μ l of YOYO and ending with 300 μ l of YOYO, the signal of EtBr increases about 4-fold. Further addition of YOYO results in a progressive but slower decrease of the EtBr signal, as predicted by the simulation shown in Figure 23. As already pointed out, with the addition of

YOYO, a small shift toward the blue for EtBr emission is observed as well, which indicates an increasing fraction of emission originating from the EtBr bound to DNA. An increase in the signal from YOYO solution begins to be observed for an addition of about 50 μ l of YOYO solution.

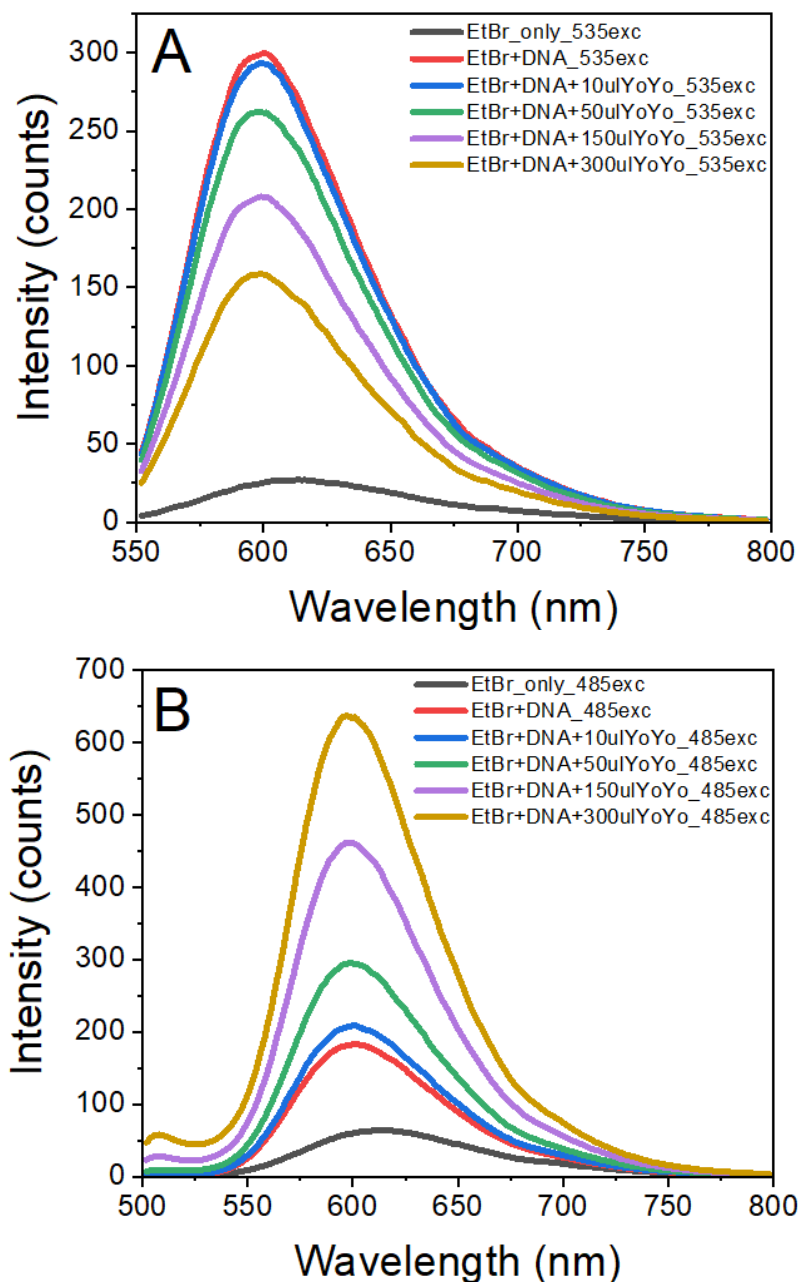


Figure 27: Emission spectra of DNA saturated EtBr and increasing amounts of YOYO, measured with 535 nm (A) and 485 nm excitation (B).

Moreover, at this point, the excitation of 535 nm starts to show a decreasing signal. The small decrease in the EtBr emission with 535 nm excitation indicates that YOYO replaces the EtBr bound to DNA and the EtBr is transferred into the solution. However, the continuous increase of the EtBr signal with 485 nm for the next few additions of YOYO is observed despite the decrease of DNA-bound EtBr fraction, indicating a dominant contribution of excitation energy transfer from YOYO.

To confirm that FRET is responsible for EtBr emission enhancement, intensity decays for YOYO (energy donor) at 520 nm observation and intensity decays at 620 nm observation that dominantly presents emission of EtBr acceptor were measured, to mimic the study conducted on DAPI (Ceresa L. 2021). Figure 28A presents fluorescence intensity decays for a free YOYO solution, a solution of YOYO with DNA, and a solution of YOYO with DNA to which increasing amounts of EtBr were added. The fluorescence lifetime for a free YOYO observed at 520 nm is very short (about 20 ps with a minor longer component). However, YOYO significantly increases its fluorescence lifetime to about 2 ns upon binding to DNA. Furthermore, consecutive additions of EtBr shorten this lifetime significantly. On the other hand, the lifetime of the solution with YOYO, EtBr, and DNA measured at 620 nm observation shows an increasing contribution from the long component, which confirms the energy transfer from YOYO to EtBr (Figure 28B).

The presented experiments unambiguously confirm that when excited with 485 nm, the high increase in the emission of EtBr is induced by FRET from the added amount of YOYO. Therefore, we can construct a spectrum that is the difference between the emission measured after the addition of YOYO and the emission measured before the addition of YOYO. Such a differential spectrum will represent the increased emission of EtBr induced by the addition of YOYO. The result of such subtraction is reported in Figure 29.

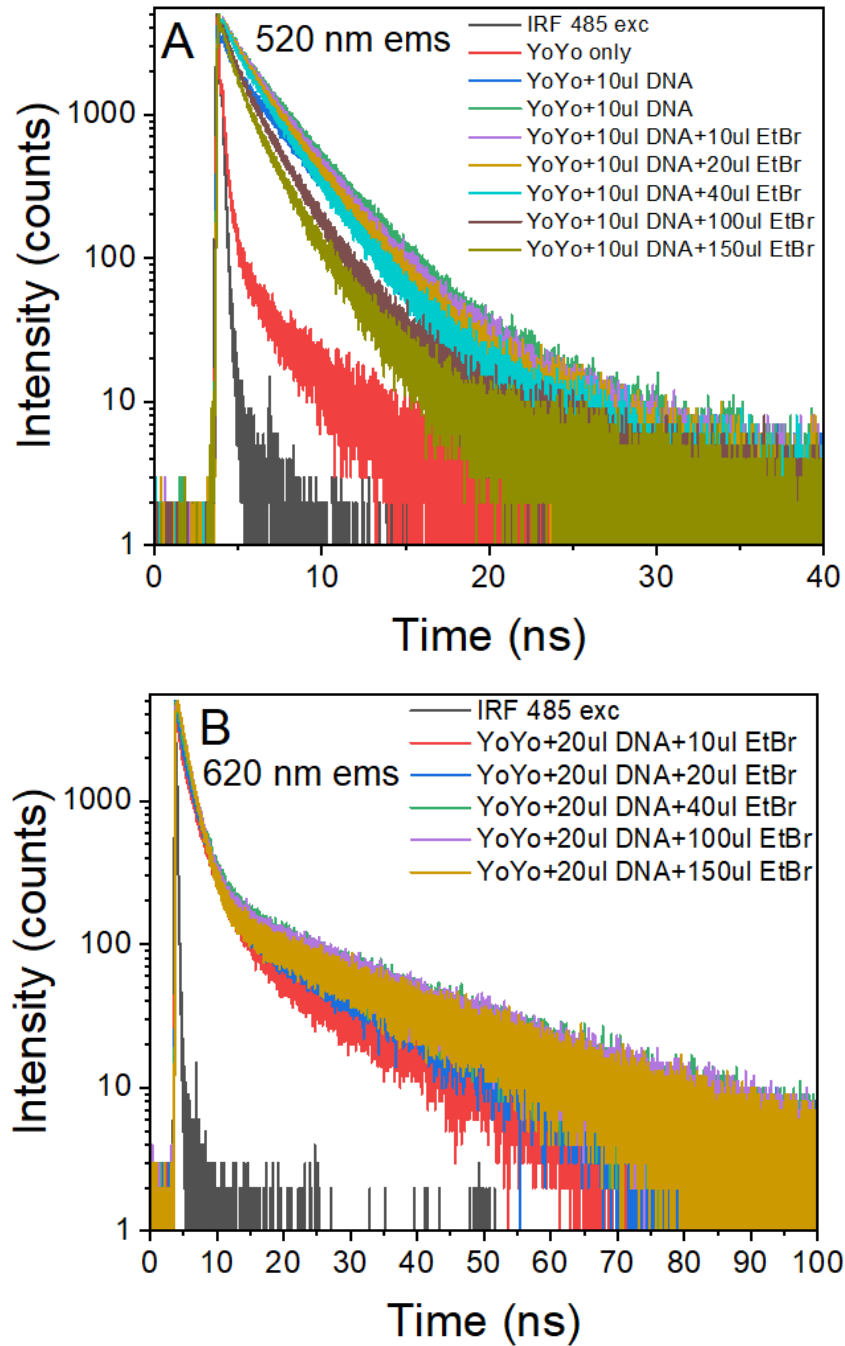


Figure 28: Fluorescence intensity decays for a free YOYO solution, a solution of YOYO with DNA, and a solution of YOYO with DNA to which we added increasing amounts of EtBr. The decays were measured at 520 nm observation (A) and 620 nm observation (B).

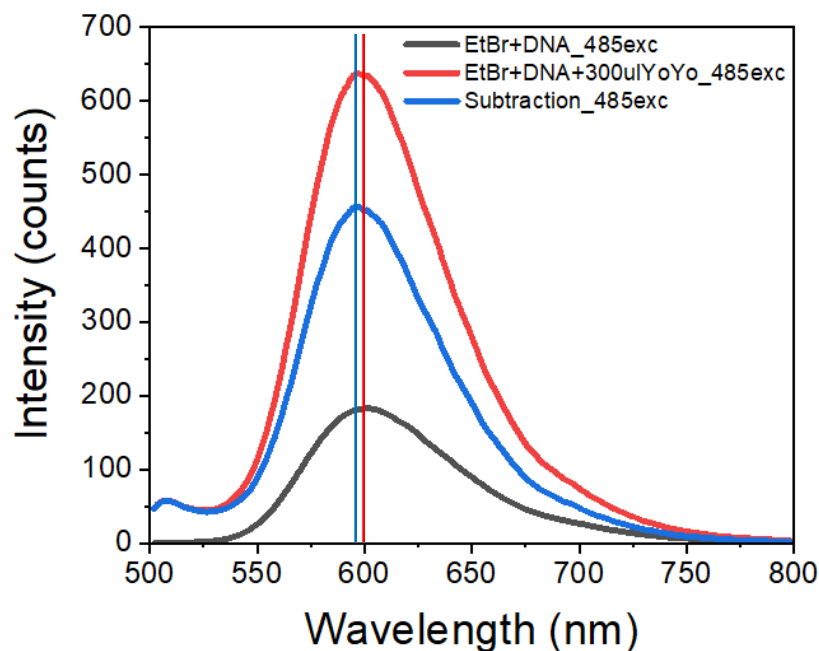


Figure 29: Emission spectra of EtBr and DNA before and after the addition of YOYO and differential spectrum.

The differential spectrum shows a clear shift towards the blue as compared to EtBr/DNA only and practically reproduces the spectrum of EtBr completely bound to DNA. This result also confirms that the energy transfer increases the contribution of DNA-bound EtBr to the overall signal. The energy transfer significantly increases the apparent fraction of EtBr bound to DNA. In other words, the effect of energy transfer from YOYO to EtBr is exclusively enabled by the presence of DNA, which works as a scaffold and accommodates the two intercalators in close proximity.

Finally, as an additional control experiment, identical amounts of EtBr and YOYO were mixed without DNA in the solution. As illustrated in Figure 30, there is no increase/change in the EtBr signal when pure EtBr is mixed with YOYO. Only upon adding DNA, we detect an increase in the measured signal from EtBr. A small spectrum modification can be seen with just 10 pg/ μ l of DNA. However, a clear signal enhancement is visible when the amount of added DNA is as low as 50

pg/ μ l. When an amount of 200 pg of DNA is added to the 1 μ l of solution, the signal of EtBr is more than doubled.

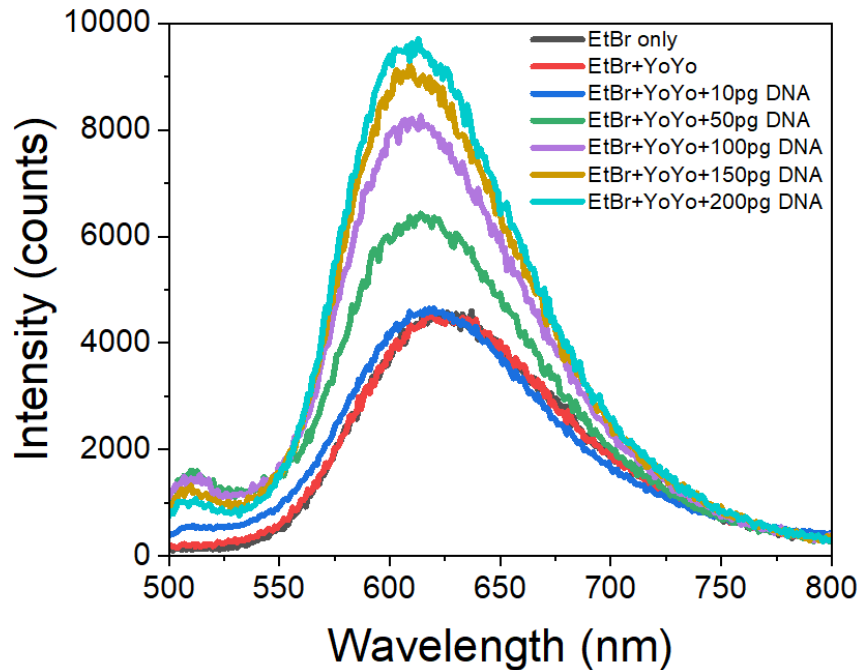


Figure 30: Emission spectra of EtBr and EtBr with YOYO with increasing amounts of DNA. In absence of DNA, the addition of YOYO causes no increase in the emission of EtBr. Since the addition of 50pg of DNA, a clear increase in the EtBr signal is visible.

To test the practical limits for DNA detection in a simple spectrophotometric setup, the standard FT300 spectrofluorometer from PicoQuant GmbH was used. This spectrofluorometer is capable of measuring emission/excitation spectra, fluorescence lifetimes, and Time-Resolved Emission Spectra (TRES). For excitation, we used a 485 nm laser diode from PicoQuant (GmbH) that can be driven with our PDL 828 "Sepia II" laser driver (PicoQuant). When using a 1 mm pathlength cuvette, the estimated excitation volume is slightly below 1 μ l. The lowest DNA concentration shown in Figure 30 was used to evaluate the potential detection limits.

The addition of 10 pg/ μ l of DNA did not produce any significant increase in the EtBr signal. In other words, the signal measured for the solution of EtBr only and the solution of EtBr with 10 pg/ μ l of DNA is very close (undistinguishable). Consequently, increasing the laser power or the detector voltage would not improve the sensitivity, and the relative signals would remain constant. However, using a burst of pulses and starting the detection with the last pulse should enhance the signal of EtBr bound to DNA that has a long (22 ns) fluorescence lifetime. The emission spectra by integrating the intensity decay after the last pulse were measured, and the results are reported in Figure 31. The measurements were done with a single pulse excitation and a burst of 4 pulses excitation for which the pulse-to-pulse separation was 12.5 ns (80 MHz repetition rate). A 5 ps time delay was applied when integrating after the last pulse to limit the excitation pulse contribution.

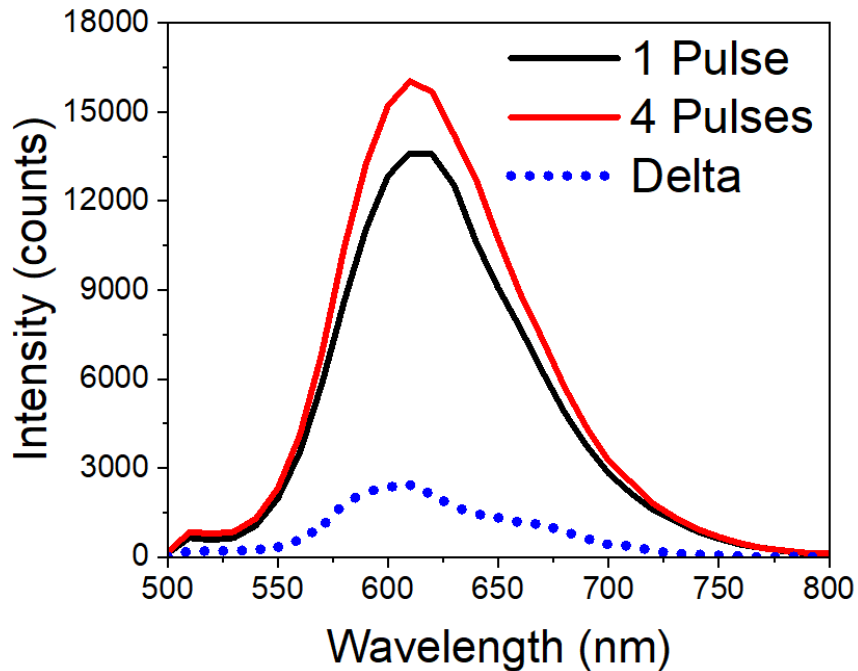


Figure 31: Time Resolved Emission Spectra (50 ps time delay to limit excitation pulse contribution) obtained from a solution of EtBr, YOYO and 10 pg/ μ l DNA with a single pulse excitation and a burst of 4 pulses for which the pulse-to-pulse separation was 12.5 ns (80 MHz rep rate). The subtraction between the signal obtained with 4 pulses and 1 pulse is displayed as a dashed line.

Figure 31 presents the emission spectra as detected with a single pulse (black line) and 4 pulses (red line) for a mixture of EtBr and YOYO with 10 pg/ μ l DNA. The intensity increase with 4 pulses is now clearly detectable. The differential emission spectrum is shown as a dashed blue line. The proposed approach readily provides detection for any higher DNA concentration. A control experiment with identical mixtures of EtBr and YOYO but no DNA added shows no increase.

Finally, YOYO and EtBr can be successfully imaged by applying the same approach of time gating and multi-pulsing. By using the same equipment described in Figure 20, we produced the photographs reported in Figure 32. Specifically, Figure 32 (A, B and C) show the emission spectra measured for solutions containing 50 pg/ μ l of DNA. The corresponding images for 1 μ l of solutions containing 50 pg/ μ l DNA placed in microwells are presented in Figure 32 (D, E, and F). Figures 32 A, 32 B, and 32 C show the spectra obtained with a solution of EtBr, a solution of EtBr and 50 pg/ μ l DNA, and a solution of EtBr and DNA to which we added either YOYO or PBS (as a control). In Figure 32A, the emission signal of EtBr, EtBr with DNA, and EtBr with DNA and 20 μ l of PBS is shown. The amount of DNA was 50 pg/ μ l, which is not detectable in the pure EtBr solution, as indicated by the drop of the red line compared to the black line. The addition of PBS causes further dilution and reduces the signal. PBS was added in order to establish a clear comparison with the addition of YOYO in the next figure (Figure 32B). Figure 32D shows two of the three wells filled with the solution of EtBr and DNA (corresponding to the signal in red in Figure 32A).

Both wells were filled with the same amount of solution (1 μ l), so a total of 50pg of DNA was present in each well. The third well was filled with PBS for comparison and did not produce visible fluorescence. Figures 32B and 32E show the effect of adding 20 μ l of YOYO to the EtBr and DNA solution.

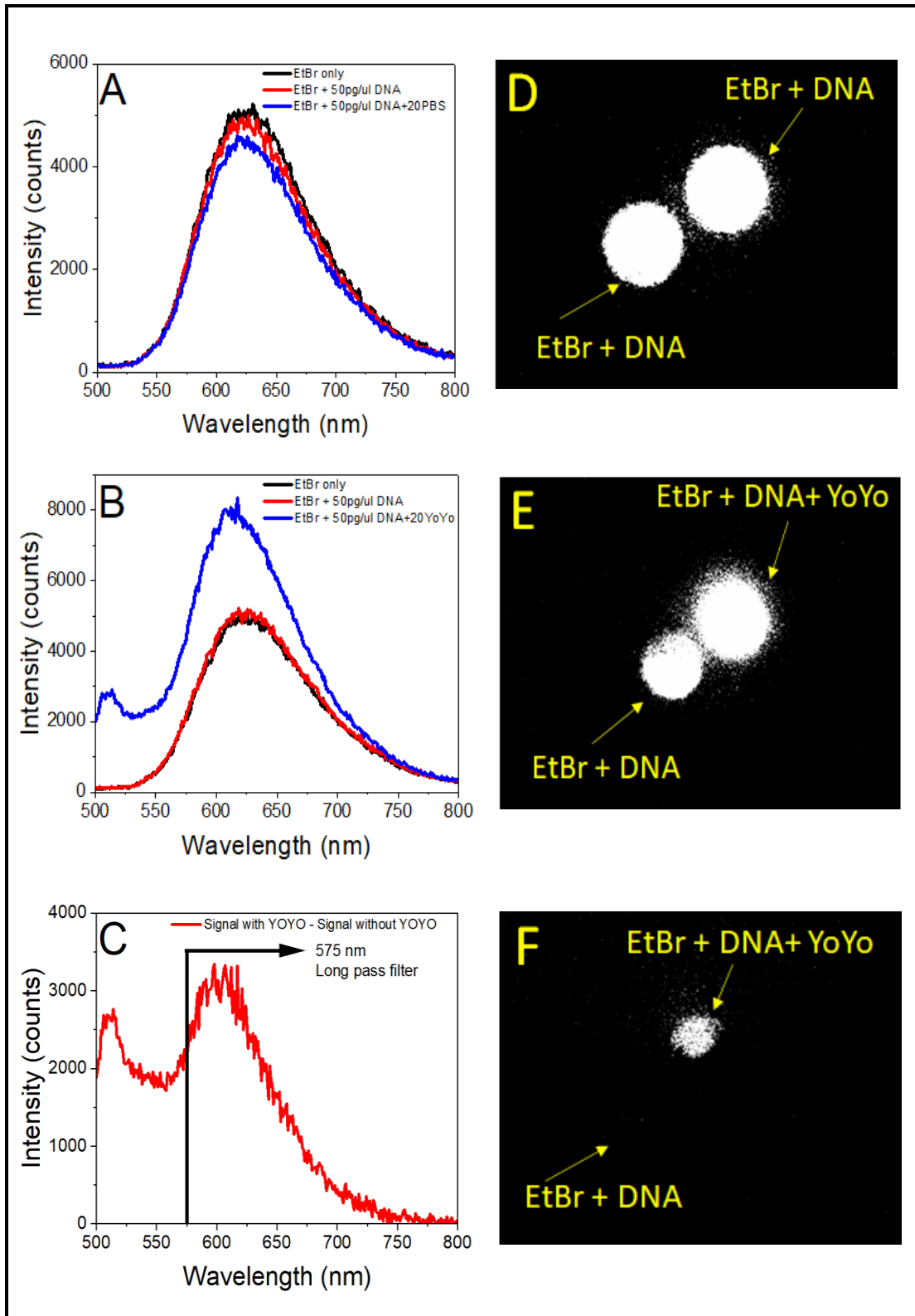


Figure 32: Emission signal of EtBr, EtBr with DNA and EtBr with DNA and 20 μ l of PBS (A); emission signal of EtBr and EtBr with DNA and 20 μ l of YOYO (B); differential signal obtained by subtraction of the signal without YOYO from the signal obtained with YOYO (C); images obtained from microwells filled with EtBr and DNA (D); images obtained from microwells filled with EtBr and DNA and EtBr with DNA and YOYO (E); differential image obtained from the subtraction of panel D from panel E (F).

The signal of YOYO appears on the left side of the spectrum (510 nm), and a clear enhancement of EtBr is detected. The Teflon cap sample holder was washed and filled with new solutions. However, the upper right well was now filled with the brighter EtBr, DNA, and YOYO solution. A 575 nm long pass filter was used so that the increase in signal is due only to an energy transfer from YOYO to EtBr and not merely to the emission of YOYO. When a simple image subtraction is performed, the image in Figure 32F is obtained. Since the signal from EtBr and DNA is the same in both images, the subtraction step completely removes the signal from this solution. However, the increase in the EtBr signal due to FRET from YOYO is visible in the image after subtraction is performed. The difference between the signals of the two solutions is reported in the plot in Figure 32C, where a 575 nm long pass filter is used in the imaging experiment.

The last experiment successfully demonstrated the capability to easily produce an image of an amount of DNA corresponding to the content of a few cells. Spectroscopically, the amount of DNA contained in a single cell can easily be detected using multi-pulsing and time-gated detection.

CONCLUSIONS

In this thesis work, we described a novel approach, that uses long fluorescence lifetimes and excitation pulse manipulation (multi-pulsing) to significantly increase the signal-to-background ratio (SBR) and greatly improve detection sensitivity. The presented approach can easily be implemented into practical tissue and microscopy imaging technologies. When combined with time-gated detection, this technique can easily achieve two orders of increase in detection sensitivity (Kimball J D 2018). This technology can be used with any long-lived luminophore, including potential uses of phosphorescence.

When using smart pulse manipulation and time-gated detection we can highly increase detection sensitivity. We presented a study focused on DNA detection with the aim of enabling detection of as low as possible amounts of DNA for forensic applications. We demonstrated a reliable DNA detection in solution down to 10 pg of DNA. This opens a possibility for detecting traces of DNA directly on substrates/surfaces or on swabs.

One of the fundamental challenges for DNA typing in forensic and diagnostic applications is collecting a sufficient amount of uncontaminated DNA for analysis. However, DNA is not visible to the human eye and its collection is typically a guessing process of whether and where DNA is present. Therefore, methods that can enhance localization and thus subsequent efficient collection of DNA from various complex substrates are of tremendous importance. In addition to potentially being able to triage swabs and other materials in the field (an advancement for better collection, efficiency, reduced labor, and cost; the latter two especially for the laboratory setting), there are other potential applications. For example, the standards for DNA processing of evidence samples in the USA require that the quantity of DNA must be determined. With more recent technologies utilized in forensic DNA typing, such as RAPID DNA (Hennessy 2014), (Cihlar JC 2022), the swab (containing the sample) is placed in a turnkey instrument and the DNA is processed to a full

profile automatically. While there are advantages to reducing labor, the technology does not include a DNA quantification step. With the approach described in this thesis, it may be possible to quantify the amount of DNA while housed in a swab without compromising the integrity of the DNA and thus meet the requirement for DNA processing of forensic evidence.

We demonstrated that by utilizing radiationless excitation energy transfer between intercalating dyes, detection sensitivity and, most importantly, specificity for DNA detection can be significantly increased. When using an energy acceptor that has a long fluorescence lifetime after binding to DNA, pulse pumping can be exploited. It is beneficial to use the MPPTG approach in combination with the excitation of the donor, which greatly increases the signal of the acceptor. Since the observed signal increase is solely associated with FRET and pulse pumping, a simple procedure of spectra (or images) subtraction dramatically limits the background signal from all short-lived components (free dye in solution and physiological components), leading to a significant increase in detection sensitivity. We demonstrated using YOYO as an energy donor and EtBr as an acceptor that a spectroscopic detection of about 10 pg of DNA in a μl solution can be achieved without the need for sample purification or volume limitation. This amount of DNA is almost equivalent to that of a single human cell DNA content. When using pulsing and image subtraction, 50 pg of unprocessed DNA can be visualized just by using the far-field imaging approach. This range of sensitivity in DNA detection/visualization will greatly improve DNA collection and highly increase the efficiency of DNA processing.

Perspectives and future translations of new technology.

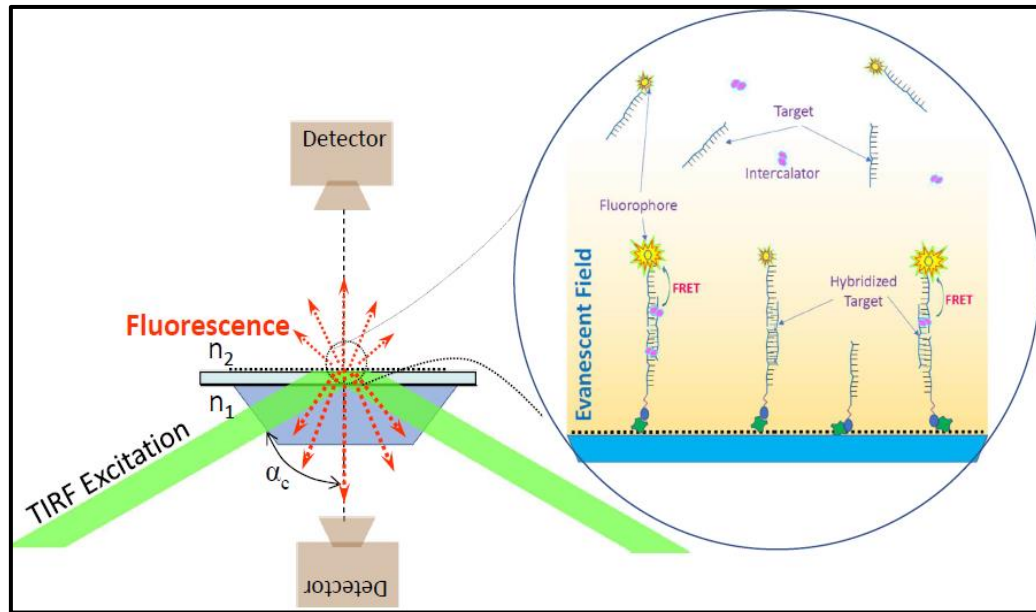


Figure 33: Left - concept of evanescent wave (TIRF) excitation. Right – concept of sandwich type DNA hybridization assay enhanced by FRET from intercalator.

Exploiting the FRET effect for enhanced DNA detection would not only improve detection sensitivity and detection specificity, but it may also have profound implications for DNA based diagnostic assays. A typical surface-confined DNA assay (so-called sandwich type assay—conceptually presented in Figure 33) is based on one DNA strand immobilized on a surface and one fluorophore-labeled strand free in solution. The sequences of both DNA strands are designed to have complementary parts to the target DNA. If targeted DNA is present in the solution, it will bind to both DNAs anchoring the labeled one to the surface. A detection format based on total internal reflection (TIRF) or surface plasmon coupled emission (SPCE) has been used by us (Malicka J 2003), (Matveeva EG. 2005), (Gryczynski I. 2004) for high-sensitivity detection. Adding an intercalator that would bind to double-stranded DNA (DNA forming a sandwich) would represent an efficient energy donor to the dye labeled to one of the DNA strands. This technique

has the potential to highly increase sensitivity and specificity for surface-confined diagnostic assays.

REFERENCES

- Betzig E, Chichester RJ. 1993. "Single molecules observed by near-field scanning optical microscopy." *Science* 1422-1425.
- Bhaumik S, Gambhir S S. 2002. "Optical imaging of Renilla luciferase reporter gene expression in living mice. ." *Proc. Natl. Acad. Sci U.S.A* 99: 377–382.
- Ceresa L, Kitchner E, Chavez J, Seung M, Bus M, Budowle B, Gryczynski I, Gryczynski Z. 2021. "A novel approach to imaging and visualization of minute amounts of DNA in small volume samples. ." *Analyst*, 146 (21): 6520-6527. doi:<https://doi.org/10.1039/D1AN013>.
- Ceresa L., Chavez J., Bus M.M., Budowle B., Kitchner E., Kimball J., Gryczynski I., Gryczynski Z. 2021. "Förster Resonance Energy Transfer-Enhanced Detection of Minute Amounts of DNA." *Anal. Chem.* 5062-5068.
- Ceresa, L., Chavez J, Kitchner E, Kimball J , Gryczynski I, Gryczynski Z. 2022. "Imaging and detection of long-lived fluorescence probes in presence of highly emissive and scattering background." *Exp. Biol. Med.* 1-12. doi:DOI: 10.1177/15353702221112121.
- Charbonnière, L J, Hildebrandt N, R. Ziessel R F, and Löhmannsröben H G. 2006. "Lanthanides to Quantum Dots Resonance Energy Transfer in Time-Resolved Fluoro-Immunoassays and Luminescence Microscopy." *J. Am. Chem. Soc.* 128: 39,: 12800–12809.
- Chib R, Requena S, Mummert M, Strzemechny Y M, Gryczynski I, Borejdo J, Gryczynski Z, Fudala R. 2016. "Fluorescence lifetime imaging with time-gated detection of hyaluronidase using a long lifetime AzaDiOxaTriAngulenium (ADOTA) fluorophore." *Methods Appl. Fluoresc.* 17;4(4): 047001.
- Cihlar JC, Kapema KB, Budowle B. 2022. "Validation of the Applied Biosystems RapidHIT ID Instrument and ACE GlobalFiler Express sample cartridge. ." *Int. J. Leg. Med.* 136(1): 13-41. doi:doi: <https://doi.org/10.1007/s00414-021-02722-9>.
- Comte J., Baechler S., Gervaix J., Lock E., Milon M.P., Delemont O., Castella V. 2019. *Forensic Sci. Int.: Genet.* 1872.
- Contag C H, Jenkins D, Contag P R, and Negrin R S. 2000. "Use of reporter genes for optical measurements of neoplastic disease in vivo. ." *Neoplasia* 2: 41–52.
- Daehne S, Resch-Genger U, Wolfbeis O S. 1998. *In Near-Infrared Dyes for High Technology Applications*. Daehne S, Ed.; Kluwer Academic Publishers: Netherlands.
- Denk W, Strickler JH, Webb, WW. 1990. "Two-photon laser scanning fluorescence microscopy." *Science* 73-76.
- Dziak R, Peneder A, Buetter A, Hageman C. 2018. "Trace DNA sampling success from evidence items commonly encountered in forensic casework." *J. Forensic Sci.* 63: 835–841. doi: DOI: 10.1111/1556-4029.13622.

- Efcavitch JW, Thompson JF. 2010. "Single-Molecule DNA Analysis. ." *Annu. Rev. Anal. Chem.* 109: 28. doi: DOI: 10.1146/annurev.anchem.111808.073558.
- Frangioni, J V. 2009. "The problem is background, not signal." *Molecular imaging* 8: 7290.2009.00033.
- Fritz M.P., Thomas M.J., Baehr W. and Holbrook J.J. 1972. *Proc. Natl. Acad. Sci. U. S. A.* 69: 3805-3809.
- Fudala R, Rich RM, Kimball J, Gryczynski I, Raut S, Borejdo J, Stankowska DL, Krishnamoorthy RR, Gryczynski K, Maliwal BP, Gryczynski Z. 2014. "Multiple-Pulse Pumping with Time-Gated Detection for Enhanced Fluorescence Imaging in Cells and Tissue." *Springer Series of Fluorescence* 225-239.
- Gacintov N, and Brenner H. 1989. "The triplet state as a probe of dynamics and structure in biological macromolecules. ." *Photochem. Photobiol.* 50(6): 841-858.
- Gross S, and Piwnica-Worms D. 2005. "Real-time imaging of ligand induced IKK activation in intact cells and in living mice." *Nat. Methods* 2: 607–614.
- Gryczynski I., Malicka J., Gryczynski Z., Lakowicz JR. 2004. "Radiative decay engineering 4. Experimental studies of surface plasmon-coupled directional emission." *Anal. Biochem.* 170-182.
- Gryczynski, Z. Gryczynski, I. 2020. *Practical Fluorescence Spectroscopy*. Taylor & Francis CRC Press.
- Hazlett T L, Johnson A E, and Jameson D M. 1989. "Time-Resolved Fluorescence Studies on the Ternary Complex Formed between Bacterial Elongation Factor Tu, Guanosine 5'-Triphosphate, and Phenylalanyl-tRNA^{phe}." *Biochemistry* 28: 4109-4117.
- Hennessy LK, Mehendale N, Chear K, Jovanovich S, Williams S, Park C, Gangano S. 2014. "Developmental validation of the GlobalFiler express kit, a 24-marker STR assay, on the RapidHIT System." *Forensic Sci. Int. Genet.* 247-258.
- Hennessy, LK, Mehendale N, Chear K, Jovanovich S, Williams S, Park C, Gangano S. 2014. "Developmental validation of the GlobalFiler express kit, a 24-marker STR assay, on the RapidHIT System." *Forensic Sci. Int. Genet.* 247-258.
- Jameson, D M. 2014. *Introduction to Fluorescence*. Taylor & Francis CRC.
- Jin D, and Piper J A. 2011. "Time-Gated Luminescence Microscopy Allowing Direct Visual Inspection of Lanthanide-Stained Microorganisms in Background-Free Condition." *Anal. Chem.* 2294–2300.
- Juris A, Balzani V, Barigelletti F, Campagna S, Belser P, Von Zelewsky A. 1988. "Ru(II) polypyridine complexes: photophysics, photochemistry, electrochemistry, and chemiluminescence." *Coord. Chem. Rev.* 84, 85-277.

- Kalayanasundarm, K. 1992. *Photochemistry of Polypyridine and Porphyrin Complexes*. . Academic Press: New York.
- Kanokwongnuwut P., Kirkbride K.P., Linacre A. 2018. *Forensic Sci. Int.: Genet.* 95.
- Kanokwongnuwut P., Kirkbride P., Linacre A. 2018. *Forensic Sci Int* 115: 291.
- Kenry C C, Liu B. 2019. "Enhancing the performance of pure organic room temperature phosphorescent luminophores." *Nat. Comm.* 10: 2111.
- Kimball J D, Maliwal B, Raut S, Doan H, Nurekeyev Z, Gryczynski I, Gryczynski Z. 2018. "Enhanced DNA detection using a multiple pulse pumping scheme with time-gating (MPPTG)." *Analyst* 143 (12): 2819-2827.
- Kitchner E, Chavez J, Ceresa L, Bus M, Budowle B, Gryczynski Z. 2021. "A novel approach for visualization and localization of small amounts of DNA on swabs to improve DNA collection and recovery process." *Analyst* 1198-1206.
- Lakowicz, J R. 2006. *Principles of Fluorescence Spectroscopy 3rd edition*. Springer Science.
- Leif R, Clay S P, Gratzner H G, Haines H G, Rao K V, Vallarino L M. 1976. "The Automation of Uterine Cancer Cytology." In *Tutorials of Cytology*, by G. L., Bahr, G. F., Bartels, P. H Wied, 313-344. Chicago, IL.
- Liu Y, Tu D, Zhu H, Ma E, Chen X. 2013. "Lanthanide-doped luminescent nano-bioprobes: from fundamentals to biodetection." *Nanoscale* 5: 1369-1384.
- Malicka J, Gryczynski I, Gryczynski Z, Lakowicz JR. 2003. "DNA Hybridization Using Surface Plasmon-Coupled Emission." *Analytical Chemistry* 6629-6633.
- Maliwal B P, Fudala R, Raut S, Kokate R, Sørensen T J, Laursen B W, Gryczynski Z, Gryczynski I. 2013. "Long-lived bright red emitting azaoxo-triangulenium fluorophores." *PLoS One* 7; 8(5):e63043.
- Maliwal B, Gryczynski Z, Lakowicz J. 2001. "Long-wavelength Long-Lifetime Luminophores." *Anal. Chem.* 73: 4277-4285.
- Matveeva EG, Gryczynski Z, Stewart DR, Gryczynski I. 2010. "Ratiometric FRET-based detection of DNA and micro-RNA on the surface using TIRF detection." *J. Luminescence* 698-702.
- Matveeva EG., Gryczynski Z., Malicka J., Lukomska J., Makowiek S., Berndt KW., Lakowicz JR., Gryczynski I. 2005. "Directional surface plasmon-coupled emission: Application for an immunoassay in whole blood." *Anal. Biochem.* 161-167.
- May A, Bhaumik S, Gambhir S S, Zhan C, and Yazdanfar S. 2009. "Whole-body, real-time preclinical imaging of quantum dot fluorescence with time-gated detection." *J. Biomedical Optics* 14 (6).

- Miyoshi N., Hara, K., Yokoyama, I., Tomita, G., Fukuda, M. 1988. "Fluorescence lifetime of acridine orange in sodium dodecyl sulfate premicellar solutions." *Photochem. Photobiol.* 47 (5): 685-688.
- Moerner WE, Kador L,. 1989. "Optical detection and spectroscopy of single molecules in a solid." *Physical Review Letters* 2535-2538.
- Moerner, WE, Fromm DP. 2003. "Methods of single-molecule fluorescence spectroscopy and microscopy." *Review of scientific instruments* 3597-3619.
- Murata SI, Kusba J, Piszczek G, Gryczynski I, Lakowicz JR . 2000. "Donor Fluorescence Decay Analysis for Energy Transfer in Double-Helical DNA with Various Acceptor Concentrations." *Biopolymers (Bio spectroscopy)* 57: 306-315. doi:10.1002/1097-0282(2000)57:5<306.
- Neely RK, Deen J, Hofkens J. 2011. "Optical mapping of DNA: Single-molecule-based methods for mapping ge-nomes. ." *Biopolymers* 95: 298-311. doi:DOI: 10.1002/bip.21579.
- Raut S L, Fudala R, Rich R, Kokate R A, Chib R, Gryczynski Z, Gryczynski I. 2014. "Long lived BSA Au clusters as a time gated intensity imaging probe." *Nanoscale* 6: 2594-2597.
- Rich RM, Gryczynski I, Fudala R, Borejdo J, Stankowska DL, Krishnamoorthy RR, Raut S, Maliwal BP, Shumilov D, Doan H, Gryczynski Z. 2014. "Multiple-pulse pumping for enhanced fluorescence detection and molecular imaging in tissue." *Methods* 66: 292-298.
- Rich RM., Gryczynski I., Borejdo J., Gryczynski Z. 2017. Multi-Pulse Pumping for Enhanced Fluorescence Detection and Molecular Imaging in Cells and Tissue. USA Patent US Patent # US 9612245 B2.
- Richards-Kortum R, and Sevick-Muraca E. 1996. "Quantitative optical spectroscopy for tissue diagnosis. ." *Annu. Rev. Phys. Chem* 47: 555– 606.
- Saviotti, M. and Galley,W. 1974. "Room temperature phosphorescence and the dynamic aspects of protein structure." *Proc. Natl. Acad. Sci. U.S.A.* 71(10): : 4154-4158.
- Schlyer B, Schauerte J, Steel D. and Gafni A. 1994. "Time-resolved room temperature protein phosphorescence: nonexponential decay from single emitting tryptophans." *Biophys J.* 67(3): 1192-1202.
- Sevick-Muraca, E.M. 2012. "Translation of Near-Infrared Fluorescence Imaging Technologies." *Annu. Rev. Med.* 63, : 217-231.
- Shang L, Dong S, Nienhaus G U. 2011. "Ultra-small fluorescent metal nanoclusters: Synthesis and biological applications." *Nano Today* 6: 401- 418.
- Shumilov D., Rich R.M., Gryczynski I., Raut S., Gryczynski K., Kimball J., Doan H., Sørensen T.J., Laursen B.W., Borejdo J. and Gryczynski Z. 2014. "Generating multiple-pulse bursts for enhanced fluorescence detection." *Methods Appl. Fluoresc.* 024009.

- Sorensen T J, Thyraug, E, Szabelski M, Gryczynski I, Gryczynski Z, Laursen, B W. 2013. "AzadioxaTriAnulenicum: a long fluorescence lifetime fluorophore for large biomolecule binding assay." *Methods Appl. Fluoresc.* 1: 025001(6pp).
- Soubret A, and Ntziachristos V. 2006. "Fluorescence molecular tomography in the presence of background fluorescence. ." *Phys. Med. Biol.* 51: 3983–4001.
- Strickler S J, Berg R A. 1962. "Relationship between Absorption Intensity and Fluorescence Lifetime of Molecules." *J. Chem. Phys.* 37: 814-822.
- Tyson D S, Castellano F N. 1999. "Intramolecular singlet and triplet energy transfer in a ruthenium(II) diimine complex containing multiple pyrenyl chromophores ." *J. Phys. Chem. A.* 103: 10955-10960.
- Vahrmeijer A L, Hutteman M, van der Vorst J R, van de Velde C J H, and Frangioni J V. 2013. "Image-guided cancer surgery using near-infrared fluorescence. ." *Nat. Rev. Clin. Oncol.* 10: 507–518.
- Valeur B, Berberan-Santos, MN. 2012. *Molecular Fluorescence. Principles and Applications.* Wiley-VCH Verlag GmbH & Co. KGaA.
- Zong C, Wu J, Liu M, Yang L, Yan F, Ju H. 2014. "Chemiluminescence Imaging for a Protein Assay via Proximity-Dependent DNAzyme Formation." *Anal. Chem.* 86, 19: 9939–9944.

VITA

- Personal background Luca Ceresa
Lecco, Italy
Son of Daniele Ceresa and Monica Lacasella
- Education Diploma, Liceo G. Casiraghi, Milan, Italy, 2011
Bachelor of Science, Materials Engineering and Nanotechnology,
Polytechnic University of Milan, Italy, 2014
Master of Science, Materials Engineering and Nanotechnology,
Polytechnic University of Milan, Italy, 2017
Master of Science, Materials Engineering, Instituto Superior
Tecnico, Lisbon, Portugal, 2017
Master of Science, Physics, Texas Christian University, Fort Worth,
Texas, 2020
- Experience Teaching Assistant, Texas Christian University, 2018-present
Research Assistant, Texas Christian University, 2018-present
Instructor for the Course of General Physics I with Laboratory
(10154), Texas Christian University, Fall 2022
- Peer reviewed papers
- Kimball, J., Chavez, J., Ceresa, L., Shah, S., Gryczynski, I., & Gryczynski, Z.; (2019). Non-Fluorescent filters for fluorescence detection with in-line geometry. *Methods and Applications in Fluorescence*. **7**. 037001.
 - Z. Gryczynski, J. Kimball, R. Fudala, J. Chavez, L. Ceresa, M. Szabelski, J. Borejdo, I. Gryczynski (2020). Photophysical Properties of 2-Phenylindole in Poly (vinyl alcohol) Film at Room Temperature. Enhanced Phosphorescence Anisotropy with Direct Triplet State Excitation. *Methods and Applications in Fluorescence*.
 - J. Chavez, L. Ceresa, E. Kitchner, J. Kimball, T. Shtoyko, R. Fudala, J. Borejdo, Z. Gryczynski and I. Gryczynski (2020). On the possibility of direct triplet state excitation of indole. *Journal of photochemistry and photobiology*.
 - J. Kimball, J. Chavez, L. Ceresa, E. Kitchner, Z. Nurekeyev, H. Doan, M. Szabelski, J. Borejdo, I. Gryczynski and Z. Gryczynski (2020). On the Origin and Correction for Inner Filter Effects in Fluorescence. Part I: Primary Inner Filter Effect - The Proper Approach for Sample Absorbance Correction. *Methods and Applications in Fluorescence*

- J. Chavez, J. Kimball, L. Ceresa, E. Kitchner, T. Shtoyko, R. Fudala, J. Borejdo, Z. Gryczynski, I. Gryczynski (2020). Luminescence properties of 5-Bromoindole in PVA films at room temperature: Direct triplet state excitation. *Journal of Luminescence*.
- E. Kitchner, J. Chavez, L. Ceresa, M. Bus, B. Budowle and Z. Gryczynski (2020). A novel approach for visualization and localization of small amounts of DNA on swabs to improve DNA collection and recovery process. *Analyst*.
- L. Ceresa, J. Kimball, J. Chavez, E. Kitchner, Z. Nurekeyev, H. Doan, J. Borejdo, I. Gryczynski, and Z. Gryczynski (2021). On the Origin and Correction for Inner Filter Effects in Fluorescence. Part II: Secondary Inner Filter Effect -The Proper Use of Front-Face Configuration for Highly Absorbing and Scattering Samples. *Methods and Applications in Fluorescence*.
- L. Ceresa, E. Kitchner, M. Seung, M.M. Bus, B. Budowle, J. Chavez, I. Gryczynski and Z. Gryczynski (2021). A novel approach to imaging and visualization of minute amounts of DNA in small volume samples. *Analyst*.
- J. Chavez, L. Ceresa, J. Reeks, Y. Strzhemechny, J. Kimball, E. Kitchner, Z. Gryczynski and I. Gryczynski (2022). Direct Excitation of Tryptophan Phosphorescence. A New Method for Triplet States Investigation. *Methods and Applications in Fluorescence*.
- L. Ceresa, J. Chavez, E. Kitchner, M.M. Bus, B. Budowle, J. Kimball, Z. Gryczynski and I. Gryczynski (2022). FRET Enhanced Detection of Minute Amounts of DNA. *Analytical Chemistry*.
- J. Chavez, L. Ceresa, J. Kimball, E. Kitchner, Z. Gryczynski and I. Gryczynski (2022). Room Temperature Luminescence of 5-Chloroindole. *Journal of Molecular Liquids*.
- L. Ceresa, J. Chavez, E. Kitchner, J. Kimball, I. Gryczynski, and Z. Gryczynski (2022). Imaging and Detection of Long-Lived Fluorescence Probes in Presence of Highly Emissive and Scattering Background. A New Practical Approach to Background Suppression by Multi-Pulse Pumping. *Experimental Biology and Medicine*.
- E. Kitchner, M. Seung, J. Chavez, L. Ceresa, J. Kimball, Z. Gryczynski and I. Gryczynski (2022). The Role of Observation Conditions in Fluorescence Measurements: Importance of G-Factor Correction, Magic Angle and Observation Wavelengths. *Methods and Applications in Fluorescence*.
- L. Ceresa, D. D. Ta, L. M. Edwards, J. D. Kimball, Z. K. Gryczynski and S. V. Dzyuba (2022). 8-Aminoquinoline-containing squaric acid congeners as polarity and viscosity probes. *Journal of Photochemistry & Photobiology*
- J. Chavez, L. Ceresa, E. Kitchner, D. Pham, Z. Gryczynski and I. Gryczynski (2023). Room Temperature Phosphorescence of 5-6 Benzoquinoline. *Methods and Applications in Fluorescence*.
- J. Chavez, L. Ceresa, E. Kitchner, D. Pham, Z. Gryczynski and I. Gryczynski (2023). Room Temperature Phosphorescence of 2-Aminopyridine with Direct Triplet State Excitation. *Spectrochimica Acta Part A: Molecular and Biomolecular Spectroscopy*.

ABSTRACT

A NEW APPROACH TO ENHANCE SIGNAL-BACKGROUND-RATIO BY SMART PULSE MANIPULATION AND TIME-GATED DETECTION: BREAKING THE LIMIT OF DNA DETECTION

by

Luca Ceresa

Department of Physics and Astronomy

Texas Christian University

Thesis advisor: Zygmunt (Karol) Gryczynski, PhD

Practical applications of optical biomedical imaging/diagnostics have been rapidly growing, stimulated by the promise of supreme sensitivity. Fluorescence detection has reached the ultimate sensitivity level of a single molecule, but only in highly purified samples in extremely restricted volumes (below femtoliter). These conditions are not applicable to real, unprocessed physiological samples. Detecting biological objects and physiological processes with high spatial and temporal resolution in real-world conditions remains a significant challenge. Over 15 years ago, it became obvious that the problem was neither the signal strength nor the sensitivity of the detector but the background. Unrelated physiological components in a typical biomedical sample overwhelm the desired sample signal. In practice, any sample at physiologically acceptable conditions is dominated by high scattering, high intrinsic fluorescence of physiological components, and Raman scattering of water. Therefore, achieving a good signal-to-background ratio (SBR) is a significant challenge. There are two options to increase the SBR; (1) increase the signal of the probe or (2) reduce the background signal. To increase the signal of the probe, we can increase its concentration, but this perturbs the physiological system. Instead, we can improve the brightness of fluorescent probes, which have already reached theoretical limits. Alternatively, to improve SBR, one could reduce the background contribution. This can only be done by intensive sample purification that would harshly alter the physiological conditions. For some probes that present

long fluorescence lifetimes (much longer than the lifetimes of physiological components), an experimental approach based on time-gated detection significantly increases SBR. However, a substantial part of the probe signal is also lost. This becomes a problem since long-lived probes often present very low brightness.

Herein, we present an approach that enhances the long-lived probe signal, suppresses the background, and greatly improves the SBR. We demonstrated the potential for imaging and localization of an amount of DNA equivalent to a single cell.